Mesoscale weather prediction with the RUC hybrid isentropic / terrain-following coordinate model

Accepted for publication in ***Monthly Weather Review***

5 September 2003

Stanley G. Benjamin, Georg A. Grell[1] , John M. Brown, Tatiana G. Smirnova[1]

NOAA Research -- Forecast Systems Laboratory

Boulder, Colorado

Rainer Bleck

Los Alamos National Laboratory

Los Alamos, New Mexico

---

[1] Also affiliated with Cooperative Institute for Research in the Environmental Sciences (CIRES), University of Colorado, Boulder, CO

Corresponding author: Stan Benjamin, stan.benjamin@noaa.gov, phone - 303-497-6387, fax – 303-497-7262, Mail – NOAA/FSL, 325 Broadway, R/E/FS1, Boulder, CO 80305 USA

ABSTRACT

A mesoscale atmospheric forecast model configured in a hybrid isentropic-sigma vertical coordinate and used in the NOAA Rapid Update Cycle (RUC) for operational numerical guidance is presented. The RUC model is the only quasi-isentropic forecast model running operationally in the world and is distinguished from other hybrid-isentropic models by its application at fairly high horizontal resolution (10-20 km) and a generalized vertical coordinate formulation that allows model levels to remain continuous and yet be purely isentropic well into the middle and even lower troposphere.

The RUC model is fully described in its 2003 operational version, including numerics and a set of fairly advanced physical parameterizations. The use of these parameterizations, including mixed-phase cloud microphysics and an ensemble-closure-based cumulus parameterization, is fully consistent with the RUC vertical coordinate without any loss of generality.

A series of experiments confirm that the RUC hybrid θ-σ coordinate reduces cross-coordinate transport over quasi-horizontal σ formulation. This reduction in cross-coordinate vertical transport results in less numerical vertical diffusion, and thereby improves numerical accuracy for moist reversible processes.

Finally, a forecast of a strong cyclogenesis case over the eastern United States is presented in which the RUC model produced an accurate 36-h prediction, especially in a 10-km nested version. Horizontal and vertical plots from these forecasts give evidence of detailed yet coherent structures of potential vorticity, moisture, and vertical motion.

1. Introduction

Numerical atmospheric prediction using an isentropic vertical coordinate was first introduced in 1968 (Eliassen and Raustein), and for the last 35 years, isentropic modeling has received a modest yet steady stream of research attention. Much of this work has centered on recasting atmospheric representation using this coordinate to better handle the lower boundary condition, resulting in the development of a variety of hybrid isentropic/terrain-following coordinate models (e.g., Bleck 1978, Deaven 1976, Gall 1972, Uccellini et al. 1979, Johnson et al. 1993, Bleck and Benjamin 1993, and Konor and Arakawa 1997). These efforts were all driven, at least in part, by a vision to translate the simplicity of the isentropic perspective of three-dimensional (3-D) baroclinic structures as shown by Rossby et al. (1937), Namias and others (see review by Gall and Shapiro 2000) into atmospheric modeling. While most applications of isentropic models up to this time have been in research, an exception is the Rapid Update Cycle (RUC), a regional mesoscale high-frequency data assimilation (Benjamin et al. 2003) and short-range numerical prediction system running operationally at the U.S. National Centers for Environmental Prediction (NCEP). The RUC model is also distinctive in its application at a much finer horizontal resolution (current 10-20 km) than previous isentropic models.

Isentropic-coordinate models are potentially advantageous in that they reduce vertical transport through coordinate surfaces. In these models, lateral mixing is carried out on isentropic surfaces rather than across them, meaning that no unwanted cross-isentropic mixing occurs. Spurious growth of entropy in non-θ models, resulting in a cold bias in climate applications (Johnson 1997) or lack of ensemble spread (Egger 1999), is avoided. Atmospheric variables frequently display strong contrast in statically stable layers, including wind (e.g., Shapiro 1978), water vapor (e.g., Johnson et al 1993), hydrometeors, and trace constituents (e.g., Zapotocny et al. 1997, Reames and Zapotocny 1999). Weaver et al. (2000)

show that laminar structures of ozone in polar regions are better represented with a 3-D off-line chemistry and transport model configured in isentropic coordinates than a similar model using a sigma-pressure coordinate with more vertical levels. Diabatic effects from radiative flux divergence, always present in the atmosphere, and intermittent latent heating/cooling cause departures of material flow from isentropic surfaces. However, to a first order approximation, isentropic surfaces are material surfaces in the free atmosphere. Moreover, the moisture and potential vorticity environment for areas of precipitation may be forecast with better coherence using an isentropic model (Johnson et al. 1993, Bleck and Benjamin 1993). Isentropic coordinates also have advantage in that they provide adaptive vertical resolution, greater in layers of higher static stability where strong vertical gradients of other variables are likely to occur The concentration of isentropes in frontal zones of high thermal contrast means that these zones appear as larger-scale features in both along-front and cross-front dimensions when viewed in an isentropic perspective (e.g., Dutton 1976, Benjamin 1989, Gall and Shapiro 2000). All of these advantages of isentropic modeling in the atmosphere have counterparts in isopycnal modeling in the ocean (e.g., Bleck and Boudra 1981, Bleck 2002, Drijfhout 1992). This has led over the years to a two-way technology transfer which has benefitted both fields.

The RUC numerical forecast model is an advanced version of the hydrostatic primitive equation model described by Bleck and Benjamin (1993, BB-93). Its vertical coordinate is also used in the RUC assimilation system described in Benjamin et al. (2003). The use of a generalized vertical coordinate in a numerical weather prediction model introduced in BB-93 is demonstrated again in this paper, but now in an application with much higher horizontal resolution (10-20 km compared to 100-160 km in BB-93) and increased emphasis on modeling of diabatic processes.

Here we emphasize issues in the design of hybrid isentropic models and describe experiments with the RUC model to investigate the particular issue of cross-coordinate vertical transport.

2. Design of hybrid isentropic-sigma models

Various hybrid-isentropic model schemes have been developed with the goal of retaining the advantages of isentropic representation while eliminating the main shortcoming of a pure isentropic scheme, which lies in the treatment of the planetary boundary layer or other layers where entropy is constant or even may decrease with height. While other hybrid coordinate models exist, especially hybrid sigma-pressure models with terrain-following coordinates (Phillips 1957) gradually turning into isobaric coordinates above some intermediate constant-pressure level, we limit our discussion here specifically to isentropic-sigma (θ-σ) hybrid coordinate definitions.

Bleck (1978) describes four different types of hybrid θ-σ models. All of these designs define a specific coordinate surface where σ representation near the ground makes a transition to θ representation aloft. One of these options (B), with the transition level at a fixed pressure distance above the surface, is found in the University of Wisconsin (UW) hybrid θ-σ model (Johnson et al. 1993). This model has been the basis for a number of studies that have demonstrated various numerical advantages of the hybrid coordinate representation over the pure σ representation (e.g., Johnson et al. 1993, Zapotocny et al. 1994, Johnson et al. 2000). Only one of the hybrid design options (option D) described by Bleck (1978) avoids coordinate intersections at the interface between θ and σ domains. In option D, an above-ground isentrope is specified as the lower boundary of the θ domain, with the atmosphere below that interface resolved by σ coordinates. An example of an option-D hybrid model is the global circulation model described by Zhu et al. (1992) which used a lowest pure isentropic level of 352 K, a value necessitated by the fact that observed surface potential temperatures over the Himalayas in summer reach as high as 335 K. Johnson and Yuan (1998) have developed an option-D variant of the UW hybrid global model (called a θ-η model) with a lowest pure isentropic level of 336 K.

Two other hybrid θ-σ designs have emerged since the Bleck-1978 hybrid design classification, neither of which use fixed transition levels. The first (which we label as option E) is the two-condition (isentropic, superseded by minimum layer thickness constraint) definition described by BB-93, which provides isentropic representation far closer to the ground than previous hybrid coordinate definitions. As described in BB-93, this definition marked a significant departure from previous definitions, avoided any interface level and in fact, used an equation set written for a fully generalized vertical coordinate. The BB-93 design, used in the 20-km and 10-km version of the RUC model, is derived from a hybrid-isopycnic approach in the ocean model of Bleck and Boudra (1981), of which the HYCOM (hybrid community ocean model) ocean circulation model (Bleck 2002) is a modern descendant. The details of this design are described in greater detail in section 4. Perhaps the best way to characterize the present hybrid scheme is to call it **Arbitrary Lagrangian-Eulerian** (ALE), a term originally coined by Hirt et al. (1974). Note however, that our scheme goes far beyond ALE in that it adds the element of "coordinate maintenance", i.e., the migration of coordinate surfaces toward a set of predefined target surfaces, in this case isentropes, wherever minimum thickness conditions allow.

A second, more recent hybrid θ-σ design (which we label option F) defines the vertical coordinate as a linear combination of σ (terrain-following) and θ, as described by Konor and Arakawa (1997). The Konor/Arakawa design, like option E (BB-93), has no coordinate intersections. Zhu and Schneider (1997) adopted a hybrid coordinate similar to that of Konor and Arakawa into a general circulation model and showed improvements over a σ_p version of the same model. Purser et al. (2002) have described developmental work on a hybrid-isentropic coordinate that is similar to option F but uses a constant pressure at the top, similar to the Zhu et al. (1992) option D model.

With the hybrid coordinate definition used in the RUC model (option E), coordinate surfaces more than 100-300 hPa above the surface tend to be purely isentropic. This characteristic is similar to the UW

hybrid θ-σ model (option B) but not the Konor-Arakawa hybrid model (option F) nor the UW θ-η model (option D). Thus, the RUC coordinate combines the advantages of the UW θ-σ model (isentropic coverage down to midtropospheric levels) with those of the Zhu et al. and Konor-Arakawa models (no intersecting surfaces). In resolving much of the troposphere with isentropic levels, this coordinate is desirable for the weather forecasting application of the RUC model .

Initial efforts to use a quasi-isentropic coordinate in a nonhydrostatic framework have been introduced more recently by Skamarock (1998) and He (2002). These models also use generalized vertical coordinate frameworks in which the target coordinate, based on a smoothed isentropic/sigma structure, can change with time.

3. Reduction of vertical transport in hybrid isentropic-sigma models

Among the advantages of using a largely isentropic coordinate in an atmospheric model listed in section 1, one of the most significant is the reduction in artificial numerical dispersion resulting from vertical motion across coordinate surfaces, especially oscillatory motion associated with internal gravity waves. This reduction occurs because, under adiabatic conditions, vertical advection is identically zero in grid-point space in an isentropic model since 3-D atmospheric motion is captured in two dimensions on quasi-material θ surfaces. In situations with latent heating associated with ascending saturated air, an isentropic model will have some cross-coordinate vertical advection, but this advection will be of non-oscillatory nature and will generally be smaller than in a quasi-horizontal model. The reduction of vertical dispersion in isentropic models leads to improved transport of moisture and other scalar quantities, as demonstrated in global models with horizontal resolution of well over 100 km (Johnson et al. 1993, 2000, 2002). In this paper, we investigate cross-coordinate vertical transport in a hybrid θ-σ model applied at a horizontal resolution of 20 km.

The reduction in vertical advection found in quasi-isentropic models can be illustrated in the context of an inviscid version of the hydrostatic continuity equation, which is written in generalized vertical coordinates as

$$\frac{\partial}{\partial t}\left(\frac{\Delta p}{\Delta s}\right)+\nabla_s\bullet\left(\mathbf{V}\frac{\Delta p}{\Delta s}\right)+\frac{\partial}{\partial s}\left(\dot{s}\frac{\Delta p}{\Delta s}\right)=0 \qquad (1)$$

where $\frac{\Delta p}{\Delta s}$ is the pressure thickness between two generalized vertical coordinate (s) levels and s is the vertical level index. In quasi-horizontal models, the first term of this equation is ~0, meaning that any nonzero horizontal mass flux divergence (term 2) will cause mass to be transferred between layers (term 3) to maintain specified pressures at each level. In a θ-coordinate model without diabatic effects, the last term (vertical advection) is zero, implying that layers expand and contract depending on mass flux divergence. In other words, isentropic models achieve a reduction of vertical advection by replacing the balance between terms 2 and 3 in eq. 1, which is typical of sigma or pressure coordinate models, with a balance between terms 1 and 2.

4. Numerics

In this section, we discuss the numerical techniques used in the RUC model and the specific configuration used for the 20-km version of the RUC (RUC20) implemented operationally at NCEP in April 2002.

a. Vertical grid structure

The definition of the RUC model vertical structure follows that described by Bleck and Benjamin (1993, section 2e). The RUC hybrid coordinate has terrain-following layers near the surface with isentropic layers above, as shown in Fig. 1, a vertical cross section of RUC coordinate levels from an actual case. The 20-km RUC uses 50 vertical levels, with each one assigned a reference or "target" virtual potential

temperature (θ_v) value (Table 1). The algorithm used to define vertical levels by BB-93 is applied separately in each grid column and at every model dynamical time step and consists of only about 20 lines of code. Operating on one coordinate level at a time, the algorithm uses two criteria: 1) move the coordinate surface to the pressure of where the target θ_v value is found (Table 1, the *isentropic* definition), and 2) maintain a minimum pressure spacing between coordinate surfaces starting upward from the surface (the *sigma* definition). If the pressure yielded by the isentropic criterion (1) is less than that from the sigma criterion (2), the gridpoint pressure is defined as isentropic, otherwise as terrain-following (sigma). A "cushion" function (BB-93) modifies the minimum spacing in the transition zone between σ and θ definitions to avoid discontinuities in slope between the σ and θ portions of a given coordinate surface. From this two-part criterion, a new pressure, p_{new}, is defined at each grid point in the column.

The coordinate-relative vertical velocity, $\dot{s}\frac{\partial p}{\partial s}$, can now be calculated as

$$\dot{s}\frac{\partial p}{\partial s} = \frac{(p_{new} - \hat{p})}{\Delta t} \qquad (2)$$

where Δt is the model dynamical time step and $\hat{p}$ is the pressure at the outset of the vertical regridding procedure described in the previous paragraph. The value of $\dot{s}\frac{\partial p}{\partial s}$ will be zero on all levels where θ_v at the beginning of the regridding step matches the target value. If it is not zero, a new value of θ_v is also determined, as explained in BB-93, in a manner that avoids geopotential perturbations in the grid column above.

The minimum pressure spacing in the RUC is applied only between the ground and 600 hPa and is set as 2.5, 5, 7.5, and 10 hPa in the lowest 4 layers near the surface and 15 hPa at layers above that, providing

adequate resolution of the planetary boundary layer and mixing near the surface. These minimum pressure thicknesses are reduced over higher terrain to avoid "bulges" of σ layers protruding upward in these regions (illustrated in Fig. 2).

The hybrid θ-σ algorithm used to define the 3-D pressure field in the RUC model can be replaced by a sigma-pressure (σ_p) algorithm, resulting in a σ_p version of the RUC generalized coordinate model. Table 2 contrasts the parameters which must be predefined for a θ-σ vs. a σ coordinate and the variables used in the adaptive definition of gridpoint placement in each vertical column.

The maximum θ_v value in the RUC20 is 500 K; this surface is typically found at 45-60 hPa for the operational RUC domain with a latitude range of ~15-60° N. A characteristic of the RUC hybrid coordinate is that more σ levels "pile up" near the surface in warmer areas, while more of the vertical domain is defined using isentropic surfaces in colder areas. This behavior, which is beneficial as it tends to provide high near-surface vertical resolution for convective boundary layer modeling during the warm season, and year-round at low latitudes, is apparent in Fig. 1. The case shown here is from 2 April 2002, with the cross section extending from Mississippi (on the left) northward through Wisconsin (center point), across Lake Superior (slightly higher terrain on each side), and ending in western Ontario. A frontal zone is present in the middle of the cross section, where the RUC levels (mostly isentropic) between 700 and 300 hPa are strongly sloped. In the RUC20, the isentropic levels from 270-355 K are resolved with no more than 3 K spacing (Table 1).

The adaptive variability of the generalized hybrid θ-σ coordinate used in the RUC is further explored in Fig. 2 (a west-east vertical cross section of RUC hybrid levels for a winter case) and Fig. 3. The cross section in Fig. 2, also shown in the companion paper on the RUC assimilation system (Benjamin et al. 2003), is west-east across the United States, passing south of San Francisco, through the eastern slopes of the Rocky Mountains in Colorado (where a mountain wave is evident between 300-600 hPa) and through

southern Virginia on the East Coast. Again, as in Fig. 1, the typical higher resolution using the RUC coordinate near fronts and the tropopause is apparent, as is the piling up of terrain-following levels in warmer regions (over the Pacific Ocean at the left side of the figure, in this case). A classic cold dome is evident over the central U.S., with a lowered tropopause and frontal zones extending to the surface on both sides.

Alternative perspectives of this same cross section are shown in Fig. 3, with pressure (Fig. 3a) and virtual potential temperature (Fig. 3b), both as functions of generalized coordinate level (k). These perspectives may be compared with the more familiar presentation in Fig. 2 to obtain some insights into the RUC hybrid coordinate. For instance, the θ_v vs. k cross section (Fig. 3b) shows that well over half of the generalized grid points in this depiction are resolved as isentropic levels in which $\theta_v = \theta_{v\text{-}ref}(k)$ for this winter case. The σ layer (where generalized vertical levels have been resolved as σ levels) is deepest (in k space) at this time over the Rocky Mountains due to the combination of a relatively warm air mass and the lower surface pressure together with the minimum pressure thickness constraint. The daytime boundary layer is represented in k space as nearly vertical isotherms of θ_v isopleths near the surface (Fig. 3b).

The pressure vs. k cross-section (Fig. 3a) depicts pressure thickness between k levels ($\Delta p/\Delta s$, where s is the generalized vertical coordinate using the level k), larger where isobars are closely packed. In the 'isentropic levels' where θ spacing is constant, the closeness of isobars is proportional to $\partial p/\partial \theta$. Closely packed isobars in these isentropic levels represent lower thermal stability, common in the upper troposphere, whereas more loosely spaced isobars represent 'thin' RUC layers with higher static stability. These stable layers are found in the stratosphere, and are found also at lower k levels where the tropopause is lower in the main upper-level trough associated with the cold dome located to the east (right) of the center of the cross section.

To provide a seasonal contrast in the behavior of the RUC hybrid coordinate, pressure vs. k and θ_v vs. k cross sections are presented in Fig. 4 for a summer case (25 July 2001) for the same west-east line as in Fig. 3. In this summer case, a much higher percentage of the RUC hybrid levels are resolved as terrain-following levels, about 30 out of the 50 levels (Fig. 4b). The boundary-layer depth in k space extends up to about k=30 (θ_v = 320 K from Table 1) over Colorado, but only up to approximately k=10 over most of the cross section away from the Rocky Mountains.

b. Basic governing equations

For completeness, the governing equations presented by BB-93 are repeated here with some modifications consistent with the current RUC configuration. All of these equations are written for the generalized vertical coordinate *s* and are solved on all horizontal surfaces, whether they are purely θ, purely σ, or some combination. All horizontal and temporal derivatives are evaluated on *s* surfaces.

The horizontal momentum equation is written

$$\frac{\partial \mathbf{V}}{\partial \mathrm{t}} + \nabla_s \frac{\mathbf{V}^2}{2} + (\zeta + f)k \times \mathbf{V} + \left(\dot{\mathrm{s}} \frac{\partial p}{\partial s}\right)\frac{\partial \mathbf{V}}{\partial \mathrm{p}} = -\nabla_s M + \Pi\, \nabla_s \theta + \nabla_s \bullet \left(\upsilon \nabla_s \bullet \nabla_s^2 \mathbf{V}\right) + \mathbf{F}. \quad (3)$$

In this equation, $\zeta = \left(\frac{\partial v}{\partial x}\right)_s - \left(\frac{\partial u}{\partial y}\right)_s$ is the relative vorticity, $M = \phi + \Pi\theta$ is the Montgomery potential, $\phi = gz$ is the geopotential, and $\Pi = C_p \left(\frac{p}{p_0}\right)^{\frac{R}{C_p}}$ is the Exner function. The horizontal diffusion coefficient υ is based on horizontal deformation in the wind field (Smagorinsky 1963) and is enhanced within 5 rows of lateral boundaries and in the top 3 layers as an upper-level sponge. Otherwise, if there is no deformation, no momentum diffusion is performed. The variable F represents the effects of vertical turbulent mixing (section 5.c).

The continuity equation,

$$\frac{\partial}{\partial t}\left(\frac{\partial p}{\partial s}\right)+\nabla_s \bullet\left(\mathbf{V}\frac{\partial p}{\partial s}\right)+\frac{\partial}{\partial s}\left(\dot{s}\frac{\partial p}{\partial s}\right)=\nabla_s \bullet\left(\upsilon\nabla_s \frac{\partial p}{\partial s}\right) \tag{4}$$

can also be thought of as a tendency equation for mass thickness between layers. Diffusion is applied only in the top 3 levels as part of the sponge near the top boundary.

The thermodynamic equation

$$\frac{\partial \theta_v}{\partial t}+\mathbf{V}\bullet\nabla_s\theta_v+\dot{s}\frac{\partial p}{\partial s}\frac{\partial \theta_v}{\partial p}=\nabla_s \bullet\left(\upsilon\nabla_s \bullet\nabla_s^2\theta_v\right)+\dot{\theta}_v \tag{5}$$

is solved at all points, whether or not they happen to lie on target θ_v surfaces. If there are no diabatic effects and the generalized coordinate surface is fully isentropic, this equation collapses to

$$\frac{\partial \theta_v}{\partial t}=0.$$

The source/sink term $\dot{\theta}_v$ refers to diabatic processes described in section 5.

The moisture conservation equation

$$\frac{\partial q_a}{\partial t}+\mathbf{V}\bullet\nabla_s q_a+\dot{s}\frac{\partial p}{\partial s}\frac{\partial q_a}{\partial p}=\nabla_s \bullet\left(\upsilon\nabla_s \bullet\nabla_s^2 q_a\right)+\dot{q}_a \tag{6}$$

represents advection and horizontal diffusion processes applied to several moisture variables represented generically by q_a. The symbol q_a represents mixing ratios of water vapor (q_v), cloud water (q_c), cloud ice (q_i), rain water (q_r), snow (q_s), and graupel (q_g). The cloud microphysics interactions between these variables and their source and sink terms are explained in more detail in section 5a. The full source/sink term q_a for all moisture variables has potential contributions from many of the physical parameterizations in section 5, including resolved and subgrid-scale cloud processes and turbulent mixing.

As explained in BB-93, Eqs (3) - (5) form a closed set of equations, if there is no diabatic forcing, with the addition of a hydrostatic equation and a definition of the vertical coordinate *s*. The pressure gradient term in the momentum equation (3) is written in terms of *M,* Π, and θ_v. In the σ domain near the

surface where θ_v is not constant horizontally, this pressure gradient term is defined with two terms with the attendant potential for cancellation errors. However, in the isentropic domain above the surface where θ_v is constant horizontally, the pressure gradient in the RUC model has only one term, $\nabla_s M$. Thus, it is convenient to define the hydrostatic equation with the Montgomery potential as

$$\frac{\partial M}{\partial \theta_v} = \Pi \,. \tag{7}$$

c. Time integration

The time integration of RUC model equations over a single time step may be viewed as consisting of two parts: first, the model equations are solved as if the model were a material coordinate model, and second, the vertical regridding described in section 4a is carried out. The first part begins with a forward-in-time solution of the continuity equation (4) using the flux-corrected transport algorithm of Zalesak (1979), a positive definite scheme which prevents zero or negative pressure thicknesses. In other words, the layers expand or contract based on the horizontal mass flux convergence in the second term of (4) in a manner reminiscent of material coordinates, but layer thicknesses are later readjusted based on the outcome of the regridding process (section 4a). Next, the thermodynamic equation (5) excepting vertical advection is solved forward in time. The advective form of the Smolarkiewicz (1983) positive definite advection scheme (Appendix B of BB-93) is used for the horizontal advection of θ_v and all moisture variables. The conservation equation for moisture variables (6) is then solved, also forward in time and without vertical advection. Fourth-order diffusion is applied to θ_v and water vapor mixing ratio.

At this point, new provisional values (defined with ^) are available for pressure thickness (and pressure, $\widehat{p}$, from vertical summation of the pressure thicknesses), $\widehat{\theta_v}$, and all moisture variables, $\widehat{q_a}$, based on the solutions to (4) – (6). These new values are then used as input to the physical parameterizations (mixed phase stable cloud microphysics, convective clouds, turbulent mixing, radiation

and land-surface processes) described in section 5, depending on the time splitting described in section 5e. Tendency terms from physical parameterizations are applied at this point in each time step, updating $\widehat{\theta_v}$ and $\widehat{q_a}$, but the tendencies themselves are updated only at the frequency shown in Table 3 in section 5.f. The updated $\widehat{\theta_v}$ and $\widehat{q_a}$ are used as input to the land-surface model which determines energy and moisture budgets at the surface to couple the atmospheric and soil domains. Updated values of $\widehat{p}$ and $\widehat{\theta_v}$ are then used for a re-integration of the hydrostatic equation (7) to update *M*.

The momentum equation (3) is now solved using a second-order Adams-Bashforth scheme for the horizontal advection term. The Coriolis terms for the *u* (and *v*) components are calculated using the new values of *v* (or *u*) at alternating time steps to assure that these terms are centered in time.

At this point completing Part 1 of the time integration, all of the equations have been solved in a generalized vertical coordinate, with no accounting for its specific structure. Now (Table 2), the algorithm is applied to vertically regrid all variables to the hybrid θ-σ coordinate, restoring to the minimum pressure spacing and target θ_v values described in section 4a (Part 2). Finally, values of all variables (except hydrometeors) are nudged at and near lateral boundaries toward values from some external model (the NCEP Eta model is typically used) using the Davies and Turner (1977) approach.

The horizontal grid in the RUC model is defined as the Arakawa C grid (Arakawa and Lamb 1977), in which u and v grid points are each offset from mass points to improve numerical accuracy. There is no vertical staggering, meaning that all prognostic variables are defined on the *s* coordinate full levels, rather than at half levels.

A full vertical velocity is diagnosed in the RUC model as

$$\omega = \dot{s}\frac{\partial p}{\partial s} + \left.\frac{\partial p}{\partial t}\right|_s + \mathbf{V} \bullet \nabla_s p \qquad (8)$$

where the first term is the vertical motion *through* coordinate surfaces, the second term is the vertical motion *of* the coordinate surfaces, and the third term is the vertical motion *along* coordinate surfaces. The ω diagnostic is not a part of the RUC prognostic equation set.

5. Physical parameterizations

The RUC model includes a set of parameterizations of physical processes that are generally equivalent in sophistication to those used in other operational regional models, including NCEP's Eta model (Rogers et al. 2001) and the Canadian Meteorological Centre (CMC) GEM model (Côté et al. 1998). These parameterizations are all applied column-wise without any special treatment needed for the RUC vertical coordinate, and the frequency of their application is discussed at the end of this section.

a. Mixed phase bulk cloud microphysics

The RUC model uses an updated version of the explicit mixed-phase bulk cloud microphysics originally described as the "level 4" scheme of Reisner et al. 1998 (hereafter RRB), originally applied in the NCAR (National Center for Atmospheric Research) / Penn State Mesoscale Model (MM5, Grell et al. 1994). This microphysics routine explicitly predicts the mixing ratios of cloud water (q_c , very small droplets that travel with the air), rain water (q_r , larger water drops that fall relative to the air), cloud ice (q_i, pristine or slightly rimed ice particles that are small and fall slowly), snow (q_s , larger ice crystals or aggregates of larger crystals, possibly rimed) and graupel (q_g, heavily rimed ice particles (snow pellets) or frozen raindrops (ice pellets) that are denser than snow and may fall more rapidly), as well as the number concentration of cloud ice particles (N_i). Sources, sinks, and conversion processes between these categories include representations for all the major recognized microphysical processes (Fig. 5). For example, ice nucleation and cloud condensation, deposition and riming on frozen hydrometeors, sublimation and evaporation, ice multiplication when ice particles collide with raindrops at temperatures

just below freezing, enhanced aggregation of snow crystals at temperatures near freezing, and the formation of supercooled liquid water, are all included. This explicit mixed-phase prediction is different from the diagnostic mixed-phase prediction used in the Eta-12 (Ferrier et al. 2002). In the RUC model, all six cloud/hydrometeor variables are carried as distinct predicted variables and so are advected horizontally (on the hybrid coordinate surfaces) and vertically (section 4c). Fallout of rain, snow and ice particles is considered separately from vertical advection through coordinate surfaces.

A primary motivation for introducing such a complex scheme into an operational model is to provide better guidance, via explicit prediction of supercooled liquid water, for forecasts of regions where aircraft icing is likely. The present version of the scheme is a direct outgrowth of long-term (and continuing) active collaboration with scientists at NCAR under partial sponsorship of the Federal Aviation Administration. With the paucity of comprehensive observational datasets, a crucial aspect of this work has been the use of results from a very detailed and computationally intensive bin microphysical scheme implemented in a 2-D version of MM5 (Rasmussen et al. 2002) as a sort of ground truth for evaluating the performance of prototype revisions of the present bulk scheme.

The details of the latest version of the scheme are described in Thompson et al. (2003). These represent a considerable revision from the original scheme as described in RRB and originally implemented in the RUC in April 1998. This earlier version produced unrealistic amounts of graupel and insufficient supercooled liquid water. The new version of the scheme, now operational in the RUC20, exhibits much improved predictions of supercooled liquid water, as well as of precipitation type at the ground. Continued enhancements to the RUC microphysics scheme are expected, with a focus on ice nucleation and explicit prediction of freezing drizzle in weakly forced synoptic situations.

b. Convective parameterization

A new convective parameterization (Grell and Devenyi 2002) is used in the RUC20. This

parameterization is based on a very simple convective scheme developed by Grell (1993) and discussed in more detail by Grell et al. (1994). For the RUC20 implementation, the original scheme was first expanded to include lateral entrainment and detrainment, including detrainment of cloud water and ice to the microphysics scheme discussed in the previous section. In addition, the scheme draws on uncertainties in convective parameterizations by allowing an ensemble of various closure and feedback assumptions (related to how the explicitly predicted flow modifies the parameterized convection, which in turn modifies the environment) to be used every time the parameterization is called. The four main groups of closures that are used in the RUC20 application are based on: removal of convective available potential energy (CAPE) (Kain and Fritsch 1992, Fritsch and Chappell 1980), destabilization effects (Arakawa and Schubert 1974, Grell et al. 1994), moisture convergence (Krishnamurthi et al. 1983), and low-level vertical velocity (Frank and Cohen 1987).

These four groups are then perturbed by 27 sensitive parameters related to feedback as well as strength of convection, which give a total of 108 ensemble members that contribute to the convective scheme. Output from the parameterization may be the ensemble mean, the most probable value, a probability density function as well as other statistical values (see also Grell and Devenyi 2002). Currently only the ensemble mean is fed back to the dynamic model.

The application of the Grell/Devenyi convective scheme in the RUC model also includes a removal of the negative buoyancy capping constraint at the initial time of each model forecast in areas where the GOES sounder effective cloud amount (Schreiner et al. 2001) indicates that convection may be present. This technique can aid modeled convection in starting at grid points where observed if there is positive CAPE, although it cannot create positive CAPE. In addition, an upstream dependence is introduced through relaxation of stability (convective inhibition) constraints at adjacent downstream points based on 0-5 km above ground level mean wind, and through allowing the downdraft mass flux at the previous

convective timestep to force convection at the downstream location.

c. Land surface physics

Forecasts of near-surface conditions and boundary-layer processes in the RUC model are dependent on accurate estimates of surface fluxes, and in turn, on reasonably accurate soil moisture and temperature estimates provided by the RUC land-surface model (LSM; Smirnova et al. 1997, 2000a) . The RUC LSM contains a multilevel soil model, treatment of vegetation, and a 2-layer snow model, all operating on the same horizontal grid as the atmospheric model. It solves heat and moisture transfer equations at 6 levels for each soil column together with the energy and moisture budget equations for the ground surface, and uses an implicit scheme for the computation of the surface fluxes. The energy and moisture budgets are applied to a thin layer spanning the ground surface and including both the soil and the atmosphere with corresponding heat capacities and densities (Fig. 6). (The budget formulation over a layer rather than at the skin level is one of the primary differences between the RUC LSM and LSMs in other operational models.) The RUC frozen soil parameterization considers latent heat of phase changes in soil by applying an apparent heat capacity, augmented to account for phase changes inside the soil, to the heat transfer equation in frozen soil in place of the volumetric heat capacity for unfrozen soil. The effect of ice in soil on water transport is also considered in formulating the hydraulic and diffusional conductivities.

Accumulation of precipitation at the surface, as well as its partitioning between liquid and solid phases, is provided by the mixed-phase cloud microphysics routine (see section 5a). In the RUC20, the convective parameterization (section 5b) also contributes to the snow accumulation if the surface air temperature is at or below 0°C. With or without snow cover, surface runoff occurs if the rate at which liquid phase becomes available for infiltration at the ground surface exceeds the maximum infiltration rate. The solid phase in the form of snow or graupel (treated identically by the LSM) is accumulated on the ground/snow surface to subsequently affect soil hydrology and thermodynamics of the low

atmosphere.

The most recent version of the LSM implemented in the RUC20 has a number of improvements in treatment of snow cover over those described in Smirnova et al. (2000a). It allows evolution of snow density as a function of snow age and depth, the potential for refreezing of melted water inside the snowpack, and simple representation of patchy snow through reduction of the albedo when the snow depth is small. If the snow layer is thinner than a 2-cm threshold, it is combined with the top soil layer to permit a more accurate solution of the energy budget. This strategy gives improved prediction of nighttime surface temperatures under clear conditions and melting of shallow snow cover.

In applications of the RUC LSM in current and previous versions of the RUC, volumetric soil moisture and soil temperature at the 6 soil model levels, as well as canopy water, snow depth, and snow temperature are cycled. In the RUC20, cycling of the snow temperature of the second layer (where needed) is also performed. The RUC continues to be unique among operational models in its specification of snow cover and snow water content through cycling (Smirnova et al. 2000b). The 2-layer snow model in the RUC20 improves the evolution of these fields, especially in spring time, more accurately depicting the snow melting season and spring spike in total runoff.

c. Atmospheric radiation.

The RUC model uses a variation of the atmospheric radiation package developed by Dudhia (1989) and used with MM5, with additions for attenuation and scattering by all hydrometeor types, including graupel. This scheme is a broadband scheme with separate components for longwave and shortwave radiation.

d. Turbulent mixing.

The RUC prescribes turbulent mixing at all levels, including the boundary layer, via the level-3.0

turbulence scheme of Burk and Thompson (1989), with explicit forecast of turbulent kinetic energy and three other turbulence variables. The surface layer mixing continues to be prescribed by Monin-Obukhov similarity theory, specifically the three-layer scheme described in Pan et al. (1994).

e. Time splitting for physical parameterizations

As with other mesoscale models, the RUC model gains efficiency by use of a time splitting scheme in which physical parameterizations use time steps longer than the dynamical time step. The time step used in the 20-km RUC model for each physical parameterization as of early 2003 is shown in Table 3. Tendencies to the predictive variables calculated in these parameterizations are applied at each dynamical time step, avoiding the shock that would result from applying them only when the parameterizations are evaluated.

6. Experiments on cross-coordinate vertical transport and moist reversibility using RUC with different vertical coordinate representations

Johnson (1997) documents that the aphysical sources of entropy in numerical integration include dispersion from vertical advection. As noted by Johnson, some numerical dispersion is inevitable in Eulerian calculations. Zapotocny et al. (1996, 1997a,b) and Johnson et al. (2000, 2002) document resulting nonreversibility of transport processes with diagnostic conservation tests in two different global models, the UW θ-σ hybrid model and the NCAR Community Climate Model (CCM), a σ-coordinate model. Zapotocny et al. (1996, 1997a,b) examine the ability of these models to conserve potential vorticity and extrema of a hypothetical trace constituent. Johnson et al. (2000) extend this study to examine the treatment of moist reversible processes and conservation of equivalent potential temperature (θ_e) with the same two models. In all of these studies, the key issue is the degree of cross-coordinate vertical transport causing aphysical diffusion. As shown by Johnson et al. (2000), the UW θ-σ model

conserves θ_e with greater fidelity overall at higher levels where the grid is purely isentropic than near the surface, where the solution is dominated by terrain-following numerics. Johnson et al. (2002) performed additional diagnostics on these experiments to stratify components of the errors in the UW and CCM models.

The RUC model is applied operationally at much smaller grid lengths than the UW θ-σ global model, hence, extrema of diabatic processes are much more pronounced than on a coarse scale. Moreover, its purpose is operational prediction of significant weather events often characterized by strong diabatic effects. Therefore, it is of interest to examine the behavior of cross-coordinate vertical transport and ability to conserve θ_e for moist reversible processes in the RUC model with its mesoscale application.

A set of experiments was carried out with the RUC model to investigate these issues. Alternative versions of the model were developed, one with the hybrid θ-σ coordinate definition and one using a "fixed" σ coordinate definition. The σ coordinate version of the RUC model was defined by setting an initial 3-D sigma field [σ(i,j,k)] and then forcing this field to remain fixed during the model integration. All other numerical techniques and physical parameterizations described in sections 4 and 5 were used in both versions of the model. The σ version of the RUC model is not designed to be a competitive forecast model but only to provide a controlled comparison with the θ-σ version for the experiments described in this section. To eliminate any issues from coordinate differences associated with lateral boundary conditions, all experiments were performed with constant boundary conditions. Two cases with 24-h forecasts were run, a warm-season case initialized at 1200 UTC 23 May 2000 and a cold-season case at 1200 UTC 8 February 2001.

The results from these experiments, shown in the following sections, are influenced by the degree to which grid points in the 3-D domain are resolved as isentropic or sigma levels. Figure 7 shows the proportion of the domain resolved on isentropic levels by number of grid points and by mass for the

summer and winter cases shown. This proportion can change over time, but it changed by less than 1% over 24 h in these cases, so the values at the 12-h forecast time are shown. Consistent with the structures shown in Figs. 3 and 4 and explained in section 4a, the RUC hybrid coordinate is expected to resolve more levels as isentropic in colder areas and colder seasons. Assuming an average surface pressure of 1000 hPa over the RUC domain, this implies that the average depth of the sigma domain is about 220 hPa in the cold-season case and 320 hPa in the warm-season case.

a. Cross-coordinate vertical transport

The primary diagnostic quantity examined in this first set of experiments was the mean (domain-wide) absolute value of the cross-coordinate vertical transport, $\overline{\left|\left(\dot{s}\frac{\partial p}{\partial s}\right)\right|}$ (calculated every 10 min). Three experiments were run for both the warm-season (23 May 2000) and cold-season (8 February 2001) cases:

1. hybrid isentropic-sigma with full moist and boundary-layer physics (control)
2. hybrid isentropic-sigma with no moist or boundary-layer physics
3. fixed sigma with full moist and boundary-layer physics

We first present results from the May 2000 case, which was characterized by strong convection and some severe weather (wind gusts, hail, tornadoes) stretching from New England southwestward to Oklahoma.

Averaged over the vertical levels of the model, the cross-coordinate vertical transport is clearly smaller (Fig. 8) with the quasi-isentropic coordinate (Exp. 1), about 60-70% of that from the fixed coordinate run (Exp. 3). Since the layers between adjacent σ levels in this warm-season case are somewhat thinner, on average, than those between adjacent θ levels, this ratio would be somewhat smaller still if the transport from both experiments were mass-averaged. Figure 8 also shows a peak in

cross-coordinate transport in the late afternoon (about 2300 UTC), corresponding approximately to the time of maximum surface temperature and boundary-layer depth averaged over the North American RUC domain.

Next, the cross-coordinate transport from Exp. 1 (control) is broken down into a mean value in the θ domain vs. that in the σ domain. As shown in Fig. 9, the mean absolute cross-coordinate transport is about 6-9 times larger in the σ domain than in the θ domain. It may also be noted from Fig. 9 that the late afternoon peak in cross-coordinate transport is found only in the σ domain but not in the θ domain, showing that this diurnal variation is located in the lower troposphere rather than the middle and upper troposphere which is predominantly represented isentropically.

A possible explanation for the difference in cross-coordinate transport between Exps. 1 (hybrid) and 3 (fixed) could have been a major difference in precipitation behavior. Figure 10 shows 3-h precipitation between 9-h and 12-h from the initial time for both Exps. 1 and 3, and the domain-averaged precipitation rate from both experiments as a function of time over the 24-h forecast period is depicted in Fig. 11. The 3-h precipitation (Fig. 10) shows local differences but similar patterns from the two experiments, with slightly more precipitation from the hybrid model (Exp. 1) in a band from James Bay through southern New England. The domain-averaged precipitation (Fig. 11) over the full RUC domain tracks fairly closely in the two experiments. The total (resolved plus subgrid-scale) precipitation has one maximum near 2000 UTC, 8 h into the forecast, and another at the end of the forecast period at 1200 UTC. These maxima do not correspond closely to the peak cross-coordinate transport shown in Fig. 8. Overall, this suggests that the cross-coordinate transport peak in Fig. 8 is associated with increased vertical motion in the boundary layer but not from increased precipitation at that time.

The contrast between cross-coordinate transport in the σ and θ domains is most pronounced, as might be expected, in Exp 2, from which moist and boundary-layer physics were excluded (Fig. 12). In this no-

physics run in which the only diabatic process is diffusion, the cross-coordinate transport is about 50-60 times smaller in the θ domain than in the σ domain. The absence of the 2300 UTC peak in cross-coordinate transport in Exp. 2, combined with the precipitation results shown in Figs. 10 and 11, again points to heating-induced boundary-layer vertical motion as the cause of the peak in Exp. 1.

The same set of experiments was also run for the cold-season case of 8 February 2001, with an initial time of 1200 UTC. Here, the mean absolute cross-coordinate transport in the hybrid θ-σ, averaged by levels rather than mass, was reduced by 50% over the fixed σ model (Fig. 13). The cross-coordinate transport again showed a very large reduction at the θ levels compared to σ levels, down by a factor of about 7 with full diabatic physics. When no moist or boundary-layer physics were allowed in the hybrid model run (Exp. 2), the cross-coordinate vertical transport was reduced again by a factor of 50-60 (Fig. 14), this time for a cold-season case.

b. Moist reversibility experiments

A problem in atmospheric prediction at all time scales from short-range weather prediction to climate prediction is accurate simulation of reversible processes. Zapotocny et al. (1996, 1997a,b) studied the ability of different global models, including the UW θ-σ model, to conserve equivalent potential temperature, potential vorticity versus a proxy ozone tracer variable, and extrema of this tracer variable. Johnson et al. (2000, 2002) extended this work to study the ability of these global models to conserve moist entropy, as follows. A proxy field of equivalent potential temperature (designated as $t\theta_e$) was set to initially match the actual θ_e field. Equations in the model were simplified to correspond to moist reversible isentropic processes. The proxy $t\theta_e$ variable was advected as a tracer and then compared to θ_e calculated from model fields of θ, water vapor, and pressure at forecast durations of up to 10 days.

The experiments of Johnson et al. (2000, 2002) have been repeated here for 24-h forecasts using the

limited-area RUC model, comparing the moist reversibility of the θ-σ and σ versions. Specifically, we compare the degree of conservation of θ_e. Experiments were carried out for the same warm-season and cold-season cases used for the experiments described in section 7a. As done by Johnson et al., initial values of $t\theta_e$ were calculated using the formulation of Bolton (1980). The proxy $t\theta_e$ was advected using the horizontal and vertical advection schemes described in section 4. Parameterizations for radiative, turbulent mixing, land-surface, and convective processes were turned off. The mixed-phase cloud microphysics was modified to include only water saturation and latent heating from condensation. These modifications to the RUC model to better approximate moist reversibility were applied both to the θ-σ and σ versions. Empirical frequency distributions of $\left(\theta_e - t\theta_e\right)$ were calculated for 24-h forecasts over all grid points in the model domain, and specifically at levels 10 (lower troposphere) and 40 (near tropopause) of 50 levels. The results comparing θ-σ and σ versions of the RUC model proved to be very similar to those from Johnson et al. (2000, 2002) comparing the UW θ-σ model and CCM.

For the warm-season case, the frequency distributions of $\left|\theta_e - t\theta_e\right|$ are shown in Fig. 15 for all levels combined, level 10 only, and level 40 only. With 0.1 K class intervals, the probability density function (PDF) for all levels combined (Fig.15a) reaches a mode value of about 0.5 for the θ-σ model but only about 0.1 for the σ model. There is very little difference in the frequency distribution at level 10 (Fig. 15b), which is well within the σ range over almost all of the horizontal domain for this warm-season case. At level 40 (Fig. 15c), which is resolved entirely as an isentropic level in the θ-σ model, the frequency distribution is most different, reaching over 1.0 for the hybrid model but only about 0.12 for the sigma model. These results show that the simulation of moist reversible processes is much more accurate in the RUC θ-σ model than in the RUC σ model which does not benefit from any isentropic representation and therefore has larger cross-coordinate vertical transport (section 6a).

The same frequency distributions were calculated for the cold-season case (Fig. 16), where a greater proportion of grid points are resolved as isentropic levels (Fig. 7). The improved accuracy of moist reversible processes in the RUC θ-σ model compared to the RUC σ model is even more pronounced in this case. The peak frequencies near zero are considerably higher for the θ-σ model in this case, reaching 2.0 for level 40, and even 0.25 at level 10 (compared to 0.1 for the σ model). In contrast, the peak frequencies for the σ model are about 0.1 regardless of level and regardless of season. Overall, the use of isentropic coordinates in the RUC hybrid θ-σ model results in much higher accuracy for moist reversible processes in both warm-season and cold-season simulations at 20-km resolution. The poorer conservation by the RUC σ model may be due, in part, to use of low-order vertical advection numerics. However, the experiments nevertheless confirm the much lower susceptibility to truncation errors in the θ-σ model from decreased cross-coordinate vertical transport. Moreover, the differences in accuracy reported in these mesoscale tests with the RUC model are very similar to those shown by Johnson et al. (2000, 2002) between the UW θ-σ and the CCM global models.

7. Case study

In this section, we present a brief case study of a 36-h forecast using 20-km and 10-km versions of the RUC model for a cyclogenesis case (1200 UTC 4 February – 0000 UTC 6 February 2001) along the east coast of the United States. Initial conditions for this case are provided by the RUC analysis, including application of a digital filter initialization (Benjamin et al. 2003). Lateral boundary conditions are prescribed from the operational Eta model initialized at 1200 UTC 4 February. We will concentrate on a quasi-isentropic perspective for this case, using maps of the pressure of the dynamic tropopause (defined as the first pressure, starting from the top of each column of the native hybrid θ-σ grid, at which potential vorticity (PV) drops below 2.0 PV units) as an indicator of the overall upper-level dynamics. At

the 12-h forecast (valid 0000 UTC 5 February), the tropopause pressure (Fig. 17a) shows a major wave with a slight positive tilt over the eastern U.S., with a base near the Arkansas-Louisiana border and embedded waves over Illinois and Michigan. These three features are traceable to the 24-h forecast of tropopause pressure (Fig. 17b), at which time the base of the wave is located over southern Alabama and the embedded waves are merging over the southern Appalachians. By 0000 UTC 6 February (36-h forecast, Fig. 17c), the tropopause pressure shows a pronounced negative tilt, with a classic hook of lowered tropopause now rotating north-northeastward over southern New England with a trailing wave off the North Carolina coast. The continuity of fine filamental features in the tropopause and PV in these forecasts is typical for the RUC model.

The corresponding sea-level pressure (SLP) field evolution shows a weak surface low near Chicago (not shown) at the initial time. A surface front present at this time over the Florida peninsula and extending northeastward into the Atlantic also played a role in the later development. By the 12-h forecast time (Fig. 17a), the Midwest low had drifted over Michigan without intensification. Of more significance was a 1016-hPa low off the Georgia coast, likely formed in response to latent heat release in the model forecast. By the 24-h forecast time, this surface low, now near Cape Hatteras, had become the dominant feature and had deepened to 1007 hPa. This low subsequently tracked northeastward in the forecast to southern Connecticut, deepening to 992 hPa (Figs. 17c, 18a). This position and strength was fairly close to the verifying RUC SLP analysis for 0000 UTC 6 February (Fig. 18b), which showed a 992-hPa low south of Nantucket Island, MA. The RUC forecast had tracked the low center too far to the west and had a larger envelope of cyclonic circulation than was observed. The 10-km RUC, one-way nested inside the full 20-km RUC, produced a more realistic 36-h forecast (Fig. 18c) of the cyclonic circulation over New England and a very accurate estimate of the position of the low, within 50 km.

The 36-h forecasts for the 3-h period between 2100 UTC 5 February and 0000 UTC 6 February from

the 20-km and 10-km versions of the RUC both showed significant precipitation over New England in association with the coastal low (Fig. 19a,b). These forecasts may be compared with the Stage IV gauge and radar precipitation estimate from the same 3-h period (Fig. 19c), showing that the 20-km RUC forecast too heavy precipitation over central New England and back into the upper Hudson Valley over this period. Even the 10-km RUC appeared to overestimate precipitation in southeastern NH and southern ME, but was still a better forecast.

Vertical cross sections were taken along a north-south (with respect to the grid) line through central Connecticut from the 20-km RUC 36-h forecast of θ, potential vorticity, relative humidity, and vertical velocity (Fig. 20) to give an additional 3-D perspective on the lower- and upper-level trough at this time. The three lowered tropopause undulations apparent in Fig. 20a may be matched to areas of low tropopause pressure evident in Fig. 17c, with the central extrusion associated with the surface cyclone. A center of high PV, associated with latent heat release, is evident along the surface-based front. Areas of slight negative PV are shown over the ocean in the marine boundary layer where sensible heating is occurring, and over Quebec where the absolute vorticity is slightly negative. The main wave near southern New England is also associated with dry air subsiding to its south to nearly 900 hPa (the dry slot) and nearly saturated air along the front in a plume up to almost 400 hPa (Fig. 20b). This moist air is associated with upward vertical motion up to -80 μb s^{-1} in the 36-h RUC forecast (Fig. 20c). Again, this case is presented as a demonstration of interacting dynamical and precipitation processes in the RUC model for a case with strong development.

8. Summary

The Rapid Update Cycle (RUC) model is a hybrid isentropic / terrain-following model suitable for mesoscale weather prediction, fully compatible with parameterizations of diabatic and/or subgrid-scale

processes typically used in operational models of this resolution. Here the model is applied in various tests at 20-km and 10-km resolution (as in real-time real-data applications), much higher resolution than other hybrid-isentropic models. Furthermore, the RUC model is the only hybrid θ-σ model used for operational prediction at this time.

One of the primary advantages of modeling in isentropic coordinates, reduced cross-coordinate vertical transport, is clearly demonstrated in real-data experiments shown in this paper with full diabatic physics. This vertical transport is reduced by 30-35% for a summer case and 50% for a winter case, averaged over levels. For both cases, cross-coordinate vertical transport is lower by factor of 6-9 (reduced by 84-88%) at θ levels compared to σ levels. In experiments with no diabatic effects allowed, cross-coordinate vertical transport was found to be smaller by a factor of 50-60 (reduced by 98%) at θ levels compared to σ levels for both summer and winter cases. The RUC coordinate is able to resolve levels as fully isentropic down into the midtroposphere in summer and lower troposphere in winter; this seasonal variation accounts for the larger reduction of cross-coordinate vertical transport in θ-σ versus σ versions of the RUC model in winter. A second set of experiments is carried out to consider a related question, the numerical accuracy of θ-σ and σ versions of the RUC model for moist reversible processes. These experiments confirm the results of other studies, that use of a quasi-isentropic vertical coordinate provides significant improvement in numerical accuracy in simulating these processes.

It is relevant to discuss here our perception of the weaknesses of the RUC model as currently configured. These include inaccuracies in vertical cross-coordinate transport due to use of a nonstaggered vertical grid and the fairly common presence of a large value of $\frac{\partial^2 p}{\partial s^2}$ at the interface of the theta and sigma domains despite application of the cushion function, especially when cross-coordinate vertical mixing and transport is large, such as when a daytime mixed layer extends above this interface. The

nonstaggered vertical grid in the RUC model was initially adapted for compatibility with nonstaggered data assimilation. As discussed in BB-93, it does not fully conserve potential vorticity.

Despite these possible issues, the hybrid θ-σ RUC model has been shown here to reduce vertical dispersion caused by cross-coordinate vertical transport compared to quasi-horizontal models, and thereby to improve numerical accuracy for moist reversible processes. It produced an accurate forecast with sharply defined 3-D dynamical and moisture structures for a case study at 20-km and 10-km resolution described in this paper. The companion paper by Benjamin et al. (2003) describes statistical verification of RUC forecasts from 1 h to 24 h in duration against rawinsonde and surface observations over multi-month periods. It also describes how the θ-σ vertical coordinate is used advantageously in the data assimilation problem to initialize the RUC model.

Acknowledgments. We thank our colleagues in the RUC development group at FSL as well as colleagues at NCEP/EMC and NCAR for their contributions to the development and testing of the RUC model. This work has been supported by the FAA Aviation Weather Research Program, NOAA/OAR, and the NOAA Office of Global Programs. We thank Don Johnson for fruitful discussions and Steve Koch and Nita Fullerton of FSL and Jim Wilczak of NOAA/ETL for helpful reviews. Two figures (5 and 6) are from the Cooperative Program for Operational Meteorology, Education, and Training (COMET) web site at http://www.comet.ucar/edu of the University Corporation for Atmospheric Research (UCAR), funded by the National Weather Service (© 2003 UCAR, all rights reserved). A web site on the RUC is available at http://ruc.fsl.noaa.gov.

9. References

Arakawa, A., and V.R. Lamb, 1977: Computational design of the basic dynamical processes of the UCLA general circulation model. *Methods Comput. Phys.*, **17**, 173-265.

Arakawa, A., and W.H. Schubert, 1974: Interaction of a cumulus cloud ensemble with the large scale environment, Part I. *J. Atmos. Sci*., **31**, 674-701.

Benjamin, S.G., 1989: An isentropic mesoα-scale analysis system and its sensitivity to aircraft and surface observations. *Mon. Wea. Rev*., **117**, 1586-1603.

Benjamin, S.G., D. Dévényi, S.S. Weygandt, K.J. Brundage, J.M. Brown, G.A. Grell, D. Kim, B.E. Schwartz, T.G. Smirnova, T.L. Smith, and G.S. Manikin, 2003: An hourly assimilation/forecast cycle: The RUC. *Mon. Wea. Rev*., **131**, accepted for publication.

Bleck, R., 1978: On the use of hybrid vertical coordinates in numerical weather prediction models. *Mon. Wea. Rev.,* **115**, 3097-3114.

Bleck, R., and D. Boudra, 1981: Initial testing of a numerical ocean model using a hybrid (quasi-isopycnic) vertical coordinate. *J. Phys. Oceanogr*., **11**, 755-770.

Bleck, R., and S.G. Benjamin, 1993: Regional weather prediction with a model combining terrain-following and isentropic coordinates. Part I: Model description. *Mon. Wea. Rev.,* **121**, 1770-1785.

Bleck, R., 2002: An oceanic general circulation model framed in hybrid isopycnic-Cartesian coordinates. *Ocean Mod*., **4**, 55-88.

Bolton, D., 1980: The computation of equivalent potential temperature. *Mon. Wea. Rev*., **108**, 1046-1053.

Burk, S.D., and W.T. Thompson, 1989: A vertically nested regional numerical prediction model with second-order closure physics. *Mon. Wea. Rev.*, **117**, 2305-2324.

Côté, J., S. Gravel, A. Méthot, A. Patoine, M. Roch, and A. Staniforth, 1998: The operational CMC-MRB global environmental multiscale (GEM) model. Part I: Design considerations and formulations. *Mon. Wea. Rev*., **126**, 1373-1395.

Davies, H. C., and R.E. Turner, 1977: Updating prediction models by dynamical relaxation: An examination of the technique. *Quart. J. Royal Meteor. Soc*., **103**, 225-245.

Deaven, D.G., 1976: A solution for boundary problems in isentropic coordinate models. *J. Atmos. Sci*., **33**, 1702-1713.

Drijfhout, S.Y., 1992: Ring genesis and the related heat transport. Part II: A model comparison. *J. Phys. Oceanog*., **22**, 268-285.

Dudhia, J., 1989: Numerical study of convection observed during the winter monsoon experiment using a mesoscale two-dimensional model. *J. Atmos. Sci*., **46**, 3077-3107.

Dutton, J.A., 1976*: The Ceaseless Wind*. McGraw-Hill, Inc., 579 pp.

Egger, J., 1999: Numerical generation of entropies. *Mon. Wea. Rev.*, **127**, 2211-2216.

Eliassen, A., and E. Raustein, 1968: A numerical integration experiment with a model atmosphere based on isentropic coordinates. *Meteor. Ann*., **5**, 45-63.

Ferrier, B.S., Y. Jin, Y. Lin, T. Black, E. Rogers, and G. DiMego, 2002: Implementation of a new grid-scale cloud and precipitation scheme in the NCEP Eta model. Preprints, *15th Conf. Num. Wea. Pred*., San Antonio, TX, Amer. Meteor. Soc., 280-283.

Frank, W.M., and C. Cohen., 1987: Simulation of tropical convection systems. Part I: A cumulus parameterization. *J. Atmos. Sci*., **44**, 3787-3799.

Fritsch, J.M., and C.F. Chappell, 1980: Numerical prediction of convectively driven mesoscale pressure systems, Part I: Convective parameterization. *J. Atmos. Sci*., **37**, 1722-1733.

Gall, R., 1972: *Prediction of a quasi-steady jet core with an isentropic numerical model*. Ph.D. thesis, University of Wisconsin, 121 pp. [Available from The Schwerdtfeger Library, Space Science and Engineering Center, 1225 W. Dayton St., University of Wisconsin-Madison, Madison, WI 53706]

Gall R., and M.A. Shapiro, 2000: The influence of Carl-Gustav Rossby on mesoscale weather prediction and an outlook for the future. *Bull. Amer. Meteor. Soc*., **81**, 1507-1523.

Grell, G., 1993: Prognostic evaluation of assumptions used by cumulus parameterizations. *Mon. Wea. Rev.,* **121**, 764-787.

Grell, G.A., J. Dudhia, and D.R. Stauffer, 1994: A description of the fifth-generation Penn State/NCAR Mesoscale Model (MM5). *NCAR Technical Note*, NCAR/TN-398 + STR, 138 pp.

Grell, G.A., and D. Devenyi, 2002: A generalized approach to parameterizing convection combining ensemble and data assimilation techniques. *Geophys. Res. Lett.*, **29**, 38-1-4.

He, Z., 2002: A non-hydrostatic model with a generalized vertical coordinate. Ph.D. thesis, University of Miami, Coral Gables, FL, 99 pp.

Hirt, C.W., A.A. Amsden, and J.L. Cook, 1974: An arbitrary Langrangian-Eulerian computing method for all flow speeds. J. Comput. Phys., 14, 227--253.

Johnson, D.R., T.H. Zapotocny, F.M. Reames, B.J. Wolf, and R.B. Pierce, 1993: A comparison of simulated precipitation by hybrid isentropic-sigma and sigma models. *Mon. Wea. Rev.,* **121**, 2088-2114.

Johnson, D.R., 1997: "General coldness of climate models" and the second law: Implications for modeling and earth system. *J. Climate*, **10**, 2826-2846.

Johnson, D.R., and Z. Yuan, 1998: The development and initial tests of an atmospheric model based on a vertical coordinate with a smooth transition from terrain following to isentropic coordinates. *Advances in Atmos. Sciences*, Vol., 15, No. 3, 283-299.

Johnson, D.R., A.J. Lenzen, T.H. Zapotocny, and T.K. Schaack, 2000: Numerical uncertainties in the simulation of reversible isentropic processes and entropy conservation. *J. Climate,* **13**, 3860-3884.

Johnson, D.R., A.J. Lenzen, T.H. Zapotocny, and T.K. Schaack, 2002: Numerical uncertainties in simulation of reversible isentropic processes and entropy conservation: Part II. *J. Climate*, **15**, 1777-1804.

Kain, J.S., and J.M. Fritsch, 1992: The role of the convective "trigger function" in numerical forecasts of mesoscale convective systems. *Meteor. Atmos. Phys*., **49**, 93-106.

Konor, C.S., and A. Arakawa, 1997: Design of an atmospheric model based on a generalized vertical coordinate. *Mon. Wea. Rev.,* **125**, 1649-1673.

Krishnamurti, T.N., S. Low-Nam, and R. Pasch, 1983: Cumulus parameterization and rainfall rates II. *Mon. Wea. Rev.,* **111**, 815-828.

Pan, Z.-T., S.G. Benjamin, J.M. Brown, and T.G. Smirnova, 1994: Comparative experiments with MAPS on different parameterization schemes for surface moisture flux and boundary-layer processes. *Mon. Wea. Rev.,* **122**, 449-470.

Phillips, N.A., 1957: A coordinate system having some special advantages for numerical forecasting. *J. Meteor*., **14**, 184-185.

Purser, R.J., S.K. Kar, S. Gopalakrishnan, S., 2002: A semi-lagrangian non-hydrostatic model employing a hybrid vertical coordinate. Preprints, *15th Conf. on Num. Wea. Pred*., Amer. Meteor. Soc., San Antonio, 248-251.

Rasmussen, R.M., I. Geresdi, G. Thompson, K. Manning, and E. Karplus, 2002: Freezing drizzle formation in stably stratified layer clouds: The role of radiative cooling of cloud droplets, cloud condensation nuclei, and ice initiation. *J. Atmos. Sci.,* **59**, 837-860.

Reames, F.M., and T.H. Zapotocny, 1999: Inert trace constituent transport in sigma and hybrid isentropic-sigma models. Part I: Nine advection algorithms. *Mon. Wea. Rev*., **127**, 173-187.

Reisner, J., R.M. Rasmussen, and R.T. Bruintjes, 1998: Explicit forecasting of supercooled liquid water in winter storms using the MM5 mesoscale model. *Quart. J. Roy. Meteor. Soc.*, **142**, 1071-1107.

Rogers, E. T. Black, B. Ferrier, Y. Lin, D. Parrish, and G. DiMego, 2001: Changes to the NCEP Meso Eta Analysis and Forecast System: Increase in resolution, new cloud microphysics, modified precipitation assimilation, modified 3DVAR analysis. *NOAA/NWS Technical Procedures Bulletin No. 488.* [Available at http://www.emc.ncep.noaa.gov/mmb/mmbpll/eta12tpb , National Weather Service, Office of Climate, Water, and Weather Services, 1325 East-West Highway, Silver Spring, MD 20910, also available at http://www.nws.noaa.gov/om/tpbpr.shtml]

Rossby, C.-G., and collaborators, 1937: Isentropic analysis. *Bull. Amer. Meteor. Soc*., **18**, 201-209.

Schreiner, A.J., T.J. Schmit, W.P. Menzel, 2001: Clouds based on GOES sounder data. *J. Geophys. Res*., **106** (D17), 20349-20363.

Shapiro, M.A., 1978: Further evidence of the mesoscale and turbulent structure of upper level jet stream-frontal zone systems. *Mon. Wea. Rev.,* **106**, 1100-1111.

Smagorinsky, J., 1963: General circulation experiments with the primitive equations: I. The basic experiment. *Mon. Wea. Rev*., **91**, 99-164.

Smirnova, T.G., J.M. Brown, and S.G. Benjamin, 1997: Performance of different soil model configurations in simulating ground surface temperature and surface fluxes. *Mon. Wea. Rev.*, **125**, 1870-1884.

Smirnova, T.G., J.M. Brown, S.G. Benjamin, and D. Kim, 2000a: Parameterization of cold season processes in the MAPS land-surface scheme. *J. Geoph. Res,* **105** (D3), 4077-4086.

Smirnova, T.G., S.G. Benjamin, J.M. Brown, B. Schwartz, and D. Kim, 2000b: Validation of long-term precipitation and evolved soil moisture and temperature fields in MAPS. Preprints, *15th Conf. on Hydrology,* Amer. Meteor. Soc., Long Beach, CA, 43-46.

Skamarock, W.C., 1998: A hybrid-coordinate nonhydrostatic atmospheric model. *12th Conf. on Num. Wea. Pred*., AMS, Phoenix, 232-235.

Smolarkiewicz, P., 1983: A simple positive-definite advection scheme with small implicit diffusion. *Mon. Wea. Rev*., **111**, 479-486.

Thompson, G., R.M. Rasmussen, and K. Manning, 2003: Explicit forecasts of winter precipitation using an improved bulk microphysics scheme. Part I: description and sensitivity analysis. *Mon. Wea. Rev*., submitted.

Uccellini, L.W., D.R. Johnson, and R.E. Schlesinger, 1979: An isentropic and sigma coordinate hybrid numerical model: Model development and some initial tests. *J. Atmos. Sci*., **36**, 390-414.

Weaver, C.J., A.R. Douglass, and R.B. Rood, 2000: Lamination frequencies as a diagnostic for horizontal mixing in a 3D transport model. *J. Atmos. Sci*., **57**, 247-261.

Zalesak, S.T., 1979: Fully multidimensional flux-corrected transport algorithms for fluids. *J. Comp. Physics*, **31**, 335-362.

Zapotocny, T.H., D.R. Johnson, and F.R. Reames, 1994: Development and initial test of the University of Wisconsin global isentropic-sigma model. *Mon. Wea. Rev*., **122**, 2160-2178.

Zapotocny, T.H., A.J. Lenzen, D.R. Johnson, F.M. Reames, P.A. Politowicz, and T.K. Schaack, 1996: Joint distributions of potential vorticity and inert trace constituent in CCM2 and UW θ-σ model simulations. *Geophys. Res. Lett.,* **23**, 2525-2528.

Zapotocny, T.H., D.R. Johnson, T.K. Schaack, A.J. Lenzen, F.M. Reames, P.A. Politowicz, and Z. Yuan, 1997a: Simulations of tropospheric joint distributions in the UW θ-σ model and CCM2. *Geophys. Res. Lett.,* **24**, 865-868.

Zapotocny, T.H., A.J. Lenzen, D.R. Johnson, T.K. Schaack, and F.M. Reames, 1997b: A comparison of inert trace constituent transport between the University of Wisconsin isentropic-sigma model and the NCAR community climate model. *Mon. Wea. Rev*., **125**, 120-142.

Zhu, Z., J. Thuburn, and B.J. Hoskins, 1992: A vertical finite-difference scheme based on a hybrid σ-θ-p coordinate. *Mon. Wea. Rev*., **120**, 851-862.

Zhu, Z., and E.K. Schneider, 1997: Improvement in stratosphere simulation with a hybrid σ-θ coordinate GCM. *Quart. J. Royal Meteor. Soc.,* **123**, 2095-2113.

List of table captions

Table 1. Target θ_v values (K) for the RUC20 (50 levels).

Table 2. Definition of 3-D pressure field contrasted in σ - pressure vs. θ-σ generalized vertical coordinates. Variables for which predefined values must be set are shown for each coordinate system, as well as the variables used in the adaptive definition of the 3-d pressure field.

Table 3. Frequency of calls to physical parameterizations in RUC20.

Table 1. Target θ_v values (K) for the RUC20 (50 levels).

level	**1**	**2**	**3**	**4**	**5**	**6**	**7**	**8**	**9**	**10**
θ_v	224	232	240	245	250	255	260	265	270	273
level	**11**	**12**	**13**	**14**	**15**	**16**	**17**	**18**	**19**	**20**
θ_v	276	279	282	285	288	291	294	296	298	300
level	**21**	**22**	**23**	**24**	**25**	**26**	**27**	**28**	**29**	**30**
θ_v	302	304	306	308	310	312	314	316	318	320
level	**31**	**32**	**33**	**34**	**35**	**36**	**37**	**38**	**39**	**40**
θ_v	322	325	328	331	334	337	340	343	346	349
level	**41**	**42**	**43**	**44**	**45**	**46**	**47**	**48**	**49**	**50**
θ_v	352	355	359	365	372	385	400	422	450	500

Table 2. Definition of 3-D pressure field contrasted in σ - pressure vs. θ-σ generalized vertical coordinates. Variables for which predefined values must be set are shown for each coordinate system, as well as the variables used in the adaptive definition of the 3-d pressure field.

	σ - pressure	**θ-σ generalized**
Predefined	$\sigma_p(k)$	Δp_{min}
	p_{top}	$\theta_{v-ref}(k)$
Adaptively based on		
	p_{sfc}	p_{sfc}
		θ_v

Table 3. Frequency of calls to physical parameterizations in RUC20.

Physical parameterization	RUC20 frequency (min)
Cloud microphysics	2
Convection	2
Turbulence	2
Land-surface	2
Shortwave radiation	30
Longwave radiation	60

List of figure captions

Fig. 1. Vertical cross section showing RUC native coordinate (isentropic-sigma hybrid) levels for 20-km RUC with 50 levels. Data are taken from a RUC 12-h forecast valid at 1200 UTC 2 April 2002. Cross sections are oriented from south (Mississippi) on left to north (western Ontario) on right.

Fig. 2. Vertical cross section of RUC hybrid isentropic-sigma coordinate levels for 1800 UTC 14 January 2002. Cross-section orientation is approximately west-east through California (left), Colorado (center), and the Appalachian Mountains (right).

Fig. 3. Vertical cross sections of RUC native coordinate levels with vertical axis as coordinate level (1-50), for same winter case as shown in Fig. 2. a) Pressure (contour interval – 25 hPa), b) virtual potential temperature (contour interval – 4 K).

Fig. 4. Same as Fig. 3, except for a summer case (23 May 2000 1200 UTC) instead of a winter case. Horizontal location is same as in Figs. 2 and 3, west-east across the RUC domain, through California, Colorado, and Virginia.

Fig. 5. Schematic of the mixed-phase, bulk microphysics scheme in the operational RUC20. As noted in the text, sedimentation of ice is allowed, but ice generally sublimates, or melts to become cloud water that evaporates, before reaching the ground. (Courtesy of the COMET© Program.)

Fig. 6. Schematic presentation of the surface processes in the RUC land-surface model. (Courtesy of the COMET© Program).

Fig. 7. Percentage of 3-D domain resolved as isentropic levels in RUC hybrid coordinate experiment for warm-season and cold-season cases as a function of (i,j,k) grid points and as a function of mass (accounting for variable layer thicknesses).

Fig. 8. Mean absolute cross-coordinate vertical transport ($\overline{\left|\left(\dot{s} \frac{\partial p}{\partial s} \right)\right|}$ - see text) for May 2000 Experiments 1 and 3. Units = 0.01 hPa / time step. Averaged over vertical levels (not mass-averaged).

Fig. 9. Mean absolute cross-coordinate vertical transport for May 2000 Exp 1 (control – hybrid vertical coordinate) stratified into sigma vs. theta parts of the domain and averaged over vertical levels.

Fig. 10. 3-h precipitation for 0900 – 1200 UTC 24 May 2000 for forecasts initialized at 1200 UTC 23 May. For Exp. 1 (hybrid - left) and Exp. 3 (fixed - right). Contour interval is 0.5 cm per 3 h.

Fig. 11. Averaged precipitation (resolved and sub-grid-scale) over domain for May 2000 Experiments 1 (control) and 3 (fixed sigma). Units = 0.001 mm per 10 min. Horizontal axis is time over 24-h period.

Fig. 12. Mean absolute cross-coordinate vertical transport for Exp 1 (control – hybrid including full moist and boundary-layer physics) and Exp 2 (hybrid with no moist or boundary-layer physics). Values are plotted for both sigma and theta parts of the domain and averaged over vertical levels.

Fig. 13. Same as Fig. 8, but for winter case (8 February 2001).

Fig. 14. Same as Fig. 12, but for winter experiment.

Fig. 15. Empirical relative frequency distributions, probability density function (PDF) of simulated differences of equivalent potential temperature (θ_e) and proxy θ_e from RUC θ-σ (solid) and σ (dashed) versions for 24-h forecasts from warm-season case initialized at 1200 UTC 23 May 2000. Bin width is 0.1 K, vertical axis is PDF, and horizontal axis is temperature difference in K. a) All levels combined, b) level 10 only, and c) level 40 only. Note different vertical scales for each figure.

Fig. 16. Same as Fig. 15 but for cold-season case, 24-h forecast initialized at 1200 UTC 8 February 2001.

Fig. 17. Pressure (hPa) of the dynamic tropopause (defined in text) from 20-km RUC forecast initialized at 1200 UTC 4 February 2001. a) 12-h forecast, b) 24-h forecast, c) 36-h forecast. Line through eastern part of domain is location of vertical cross sections shown in Fig. 20.

Fig. 18. Sea-level pressure (hPa) valid at 0000 UTC 6 February 2001 for a) 36-h forecast from 20-km RUC, b) analysis from 20-km RUC, c) 36-h forecast from 10-km RUC.

Fig. 19. Estimates of 3-h precipitation (mm) for 2100 UTC 5 Feb – 0000 UTC 6 February 2001 from a) 36-h forecast from 20-km RUC, b) 36-h forecast from 10-km RUC, and c) Stage IV precipitation estimate from gauge and radar data.

Fig. 20. Vertical cross sections from 36-h forecasts from 20-km RUC model along north-south line shown in Fig. 17c for potential temperature (solid lines, every 4 K) and a) potential vorticity (PVU), b) relative humidity (%), and c) vertical velocity ($\times$ 10 $\mu b\ s^{-1}$; -7 = -70 $\mu b\ s^{-1}$).

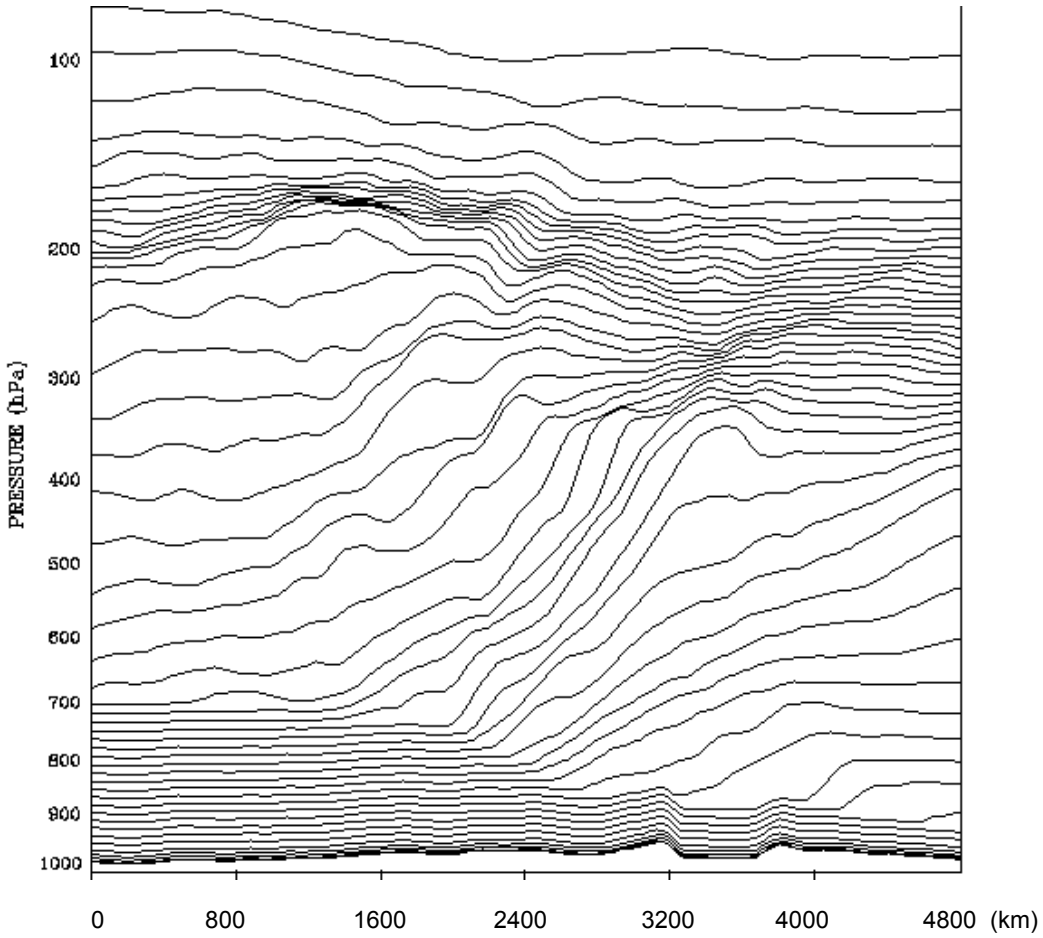

Fig. 1. Vertical cross section showing RUC native coordinate (isentropic-sigma hybrid) levels for 20-km RUC with 50 levels. Data are taken from a RUC 12-h forecast valid at 1200 UTC 2 April 2002. Cross sections are oriented from south (Mississippi) on left to north (western Ontario) on right.

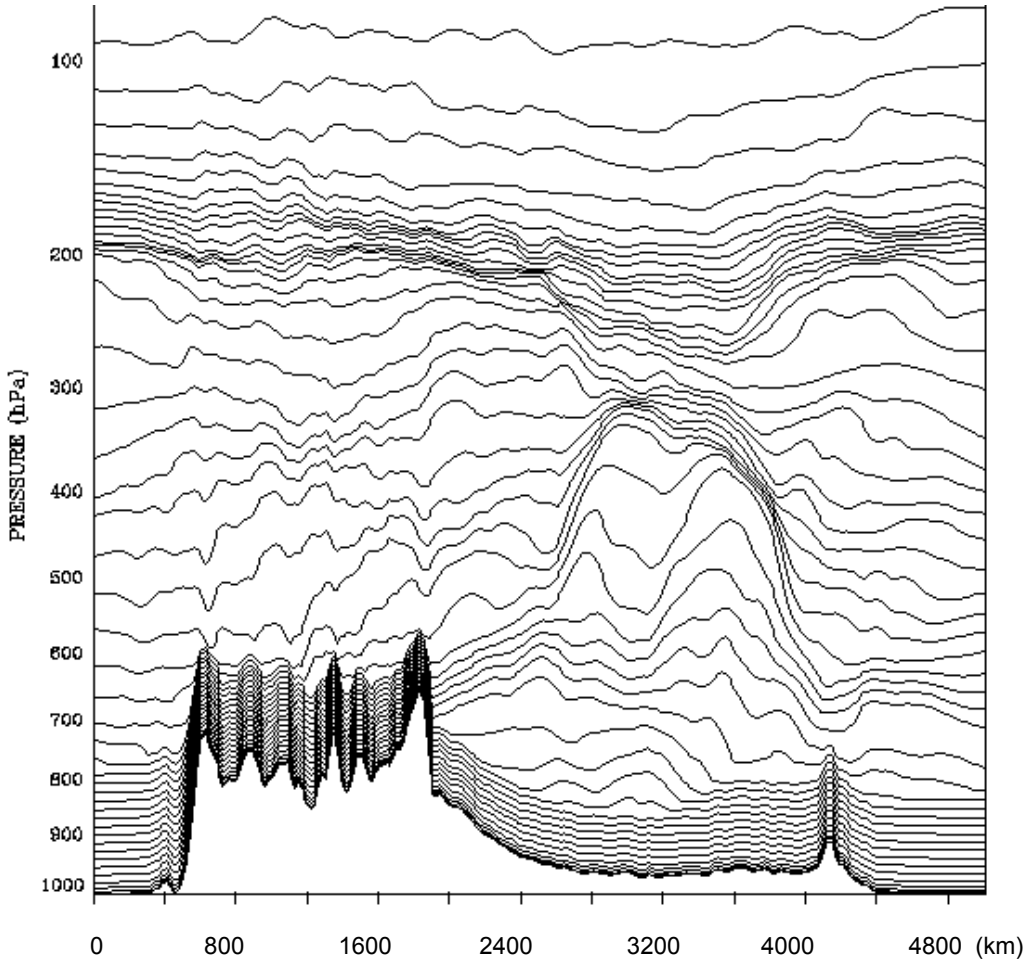

Fig. 2. Vertical cross section of RUC hybrid isentropic-sigma coordinate levels for 1800 UTC 14 January 2002. Cross-section orientation is approximately west-east through California (left), Colorado (center), and the Appalachian Mountains (right).

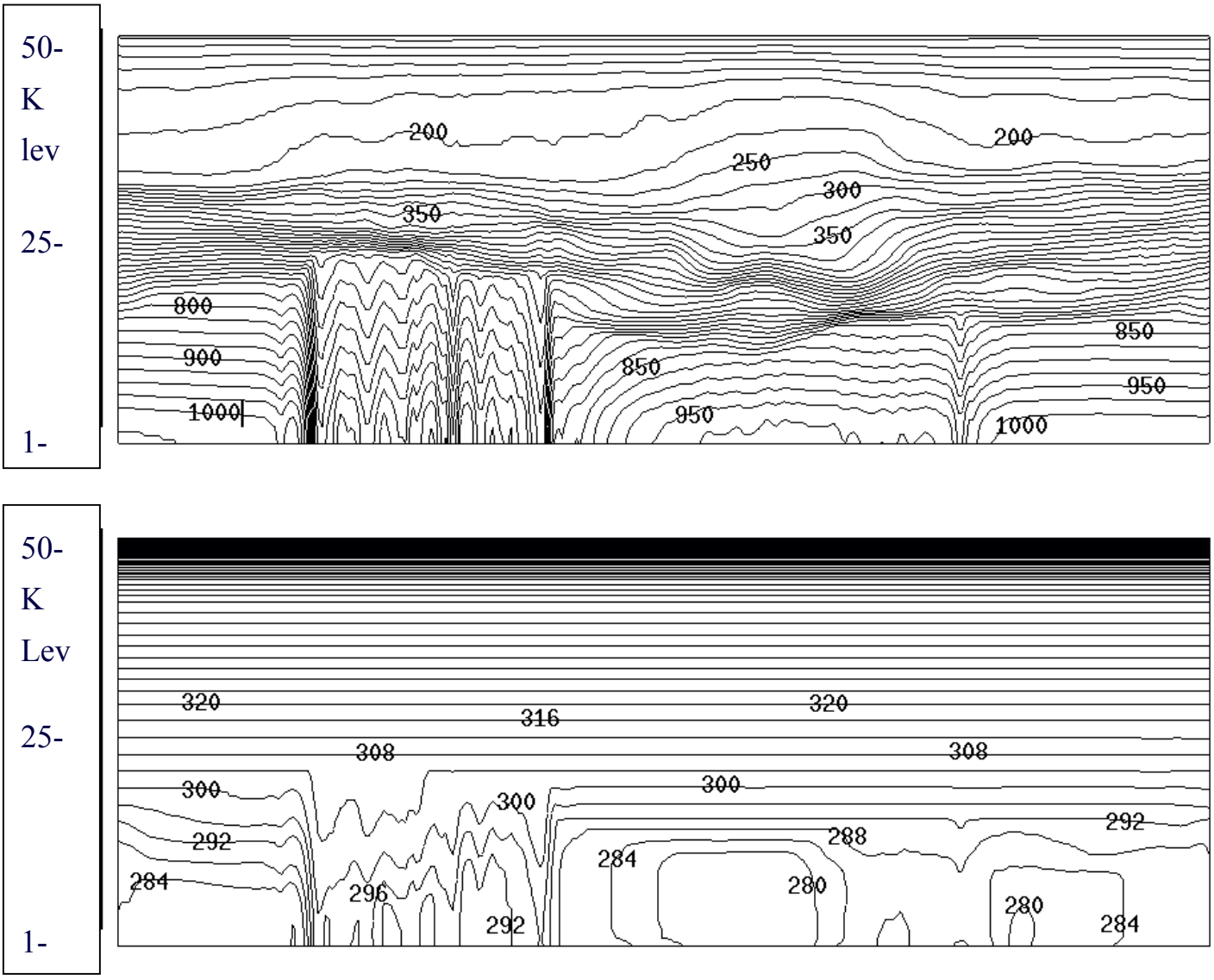

Fig. 3. Vertical cross sections of RUC native coordinate levels with vertical axis as coordinate level (1-50), for same winter case as shown in Fig. 2. a) Pressure (contour interval – 25 hPa), b) virtual potential temperature (contour interval – 4 K).

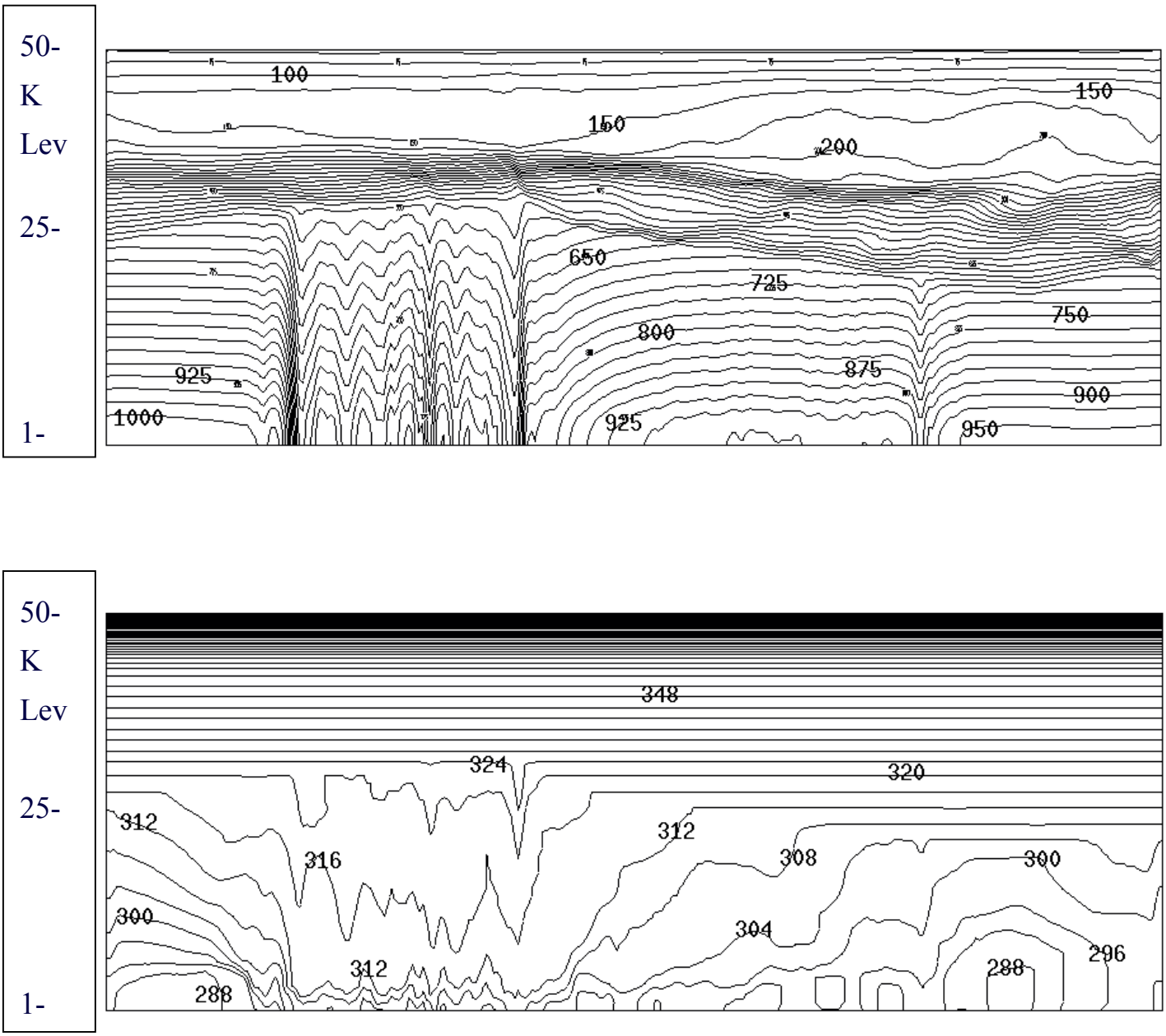

Fig. 4. Same as Fig. 3, except for a summer case (23 May 2000 1200 UTC) instead of a winter case. Horizontal location is same as in Figs. 2 and 3, west-east across the RUC domain, through California, Colorado, and Virginia.

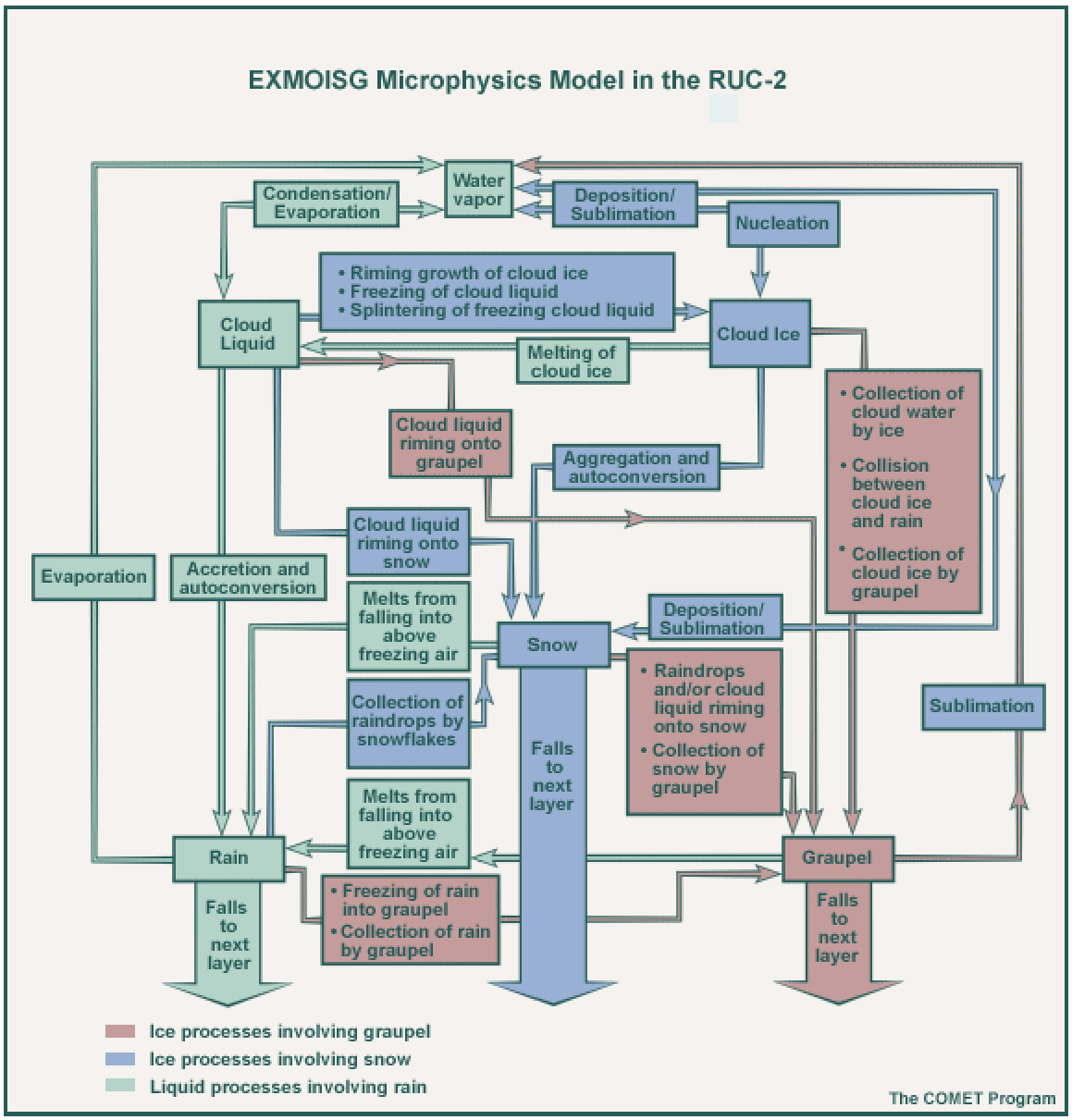

Fig. 5. Schematic of the mixed-phase, bulk microphysics scheme in the operational RUC20. As noted in the text, sedimentation of ice is allowed, but ice generally sublimates, or melts to become cloud water that evaporates, before reaching the ground. (Courtesy of the COMET© Program.)

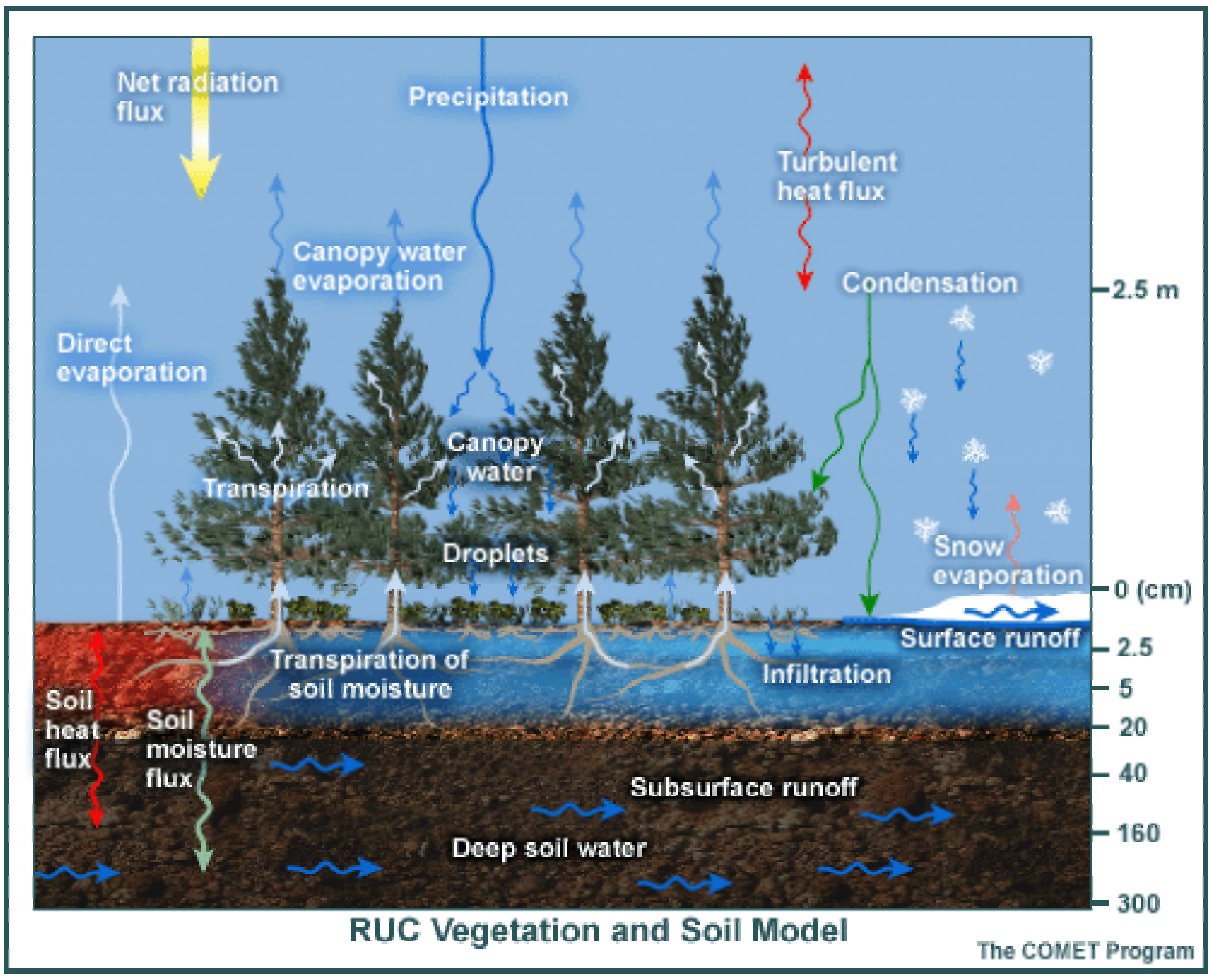

Fig. 6. Schematic presentation of the surface processes in the RUC land-surface model. (Courtesy of the COMET© Program).

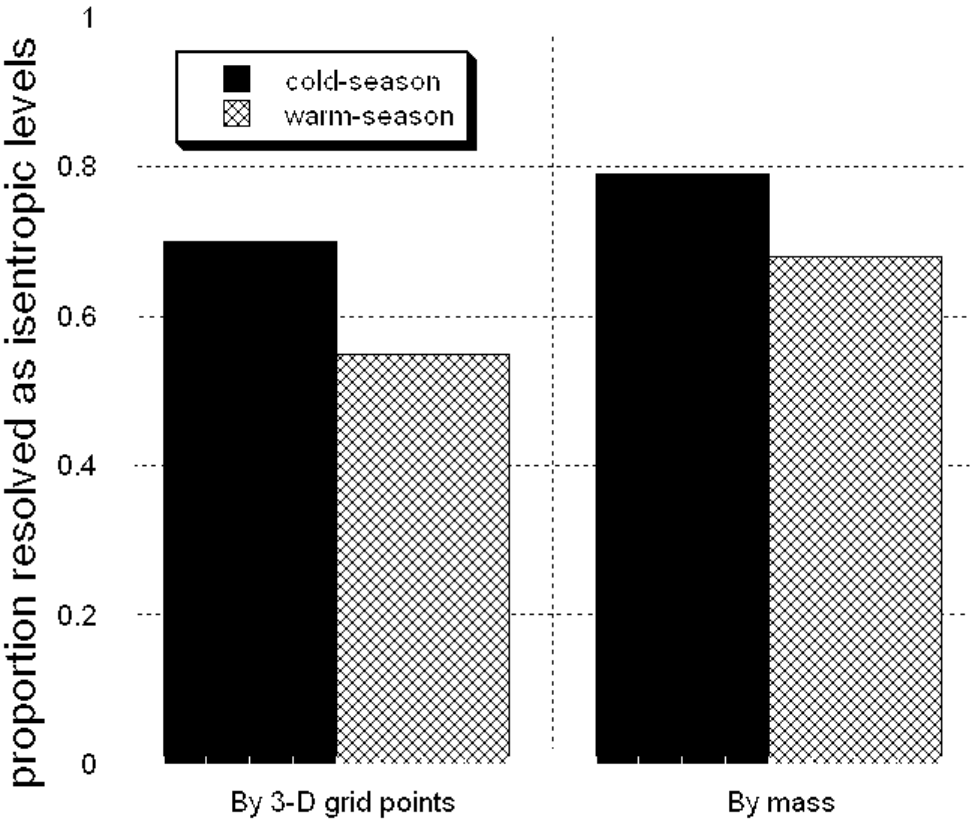

Fig. 7. Percentage of 3-D domain resolved as isentropic levels in RUC hybrid coordinate experiment for warm-season and cold-season cases as a function of (i,j,k) grid points and as a function of mass (accounting for variable layer thicknesses).

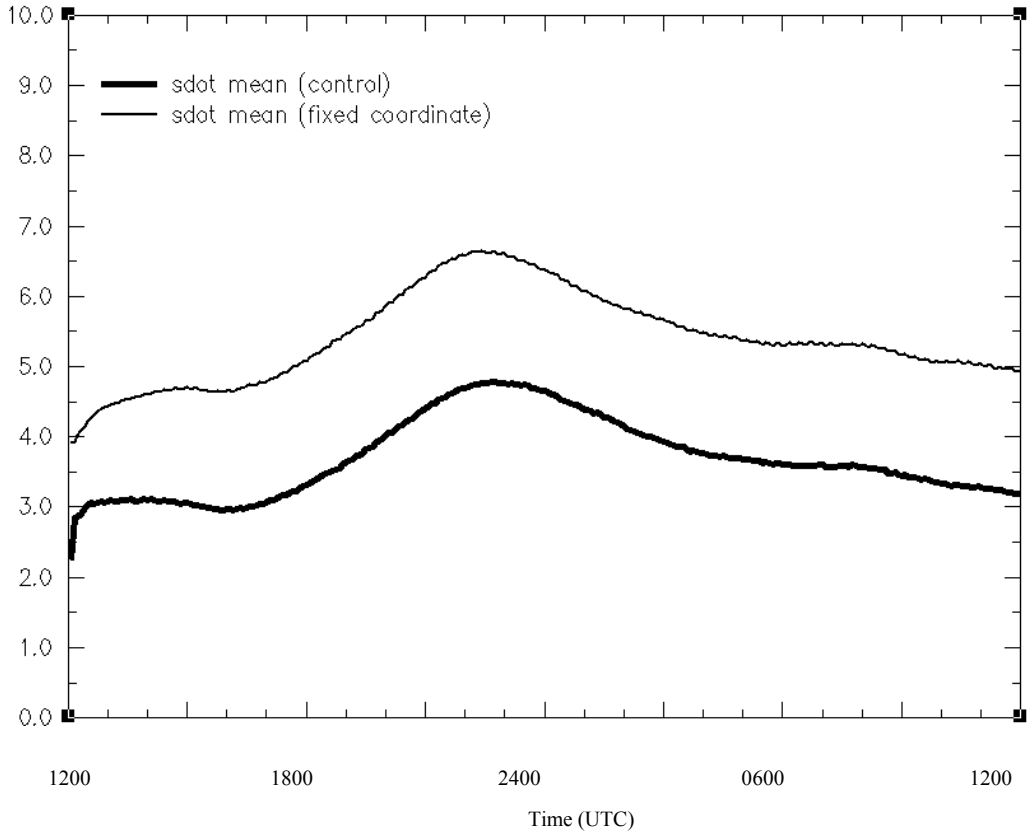

Fig. 8. Mean absolute cross-coordinate vertical transport ($\overline{\left|\left(\dot{s}\frac{\partial p}{\partial s}\right)\right|}$ - see text) for May 2000 Experiments 1 and 3. Units = 0.01 hPa / time step. Averaged over vertical levels (not mass-averaged).

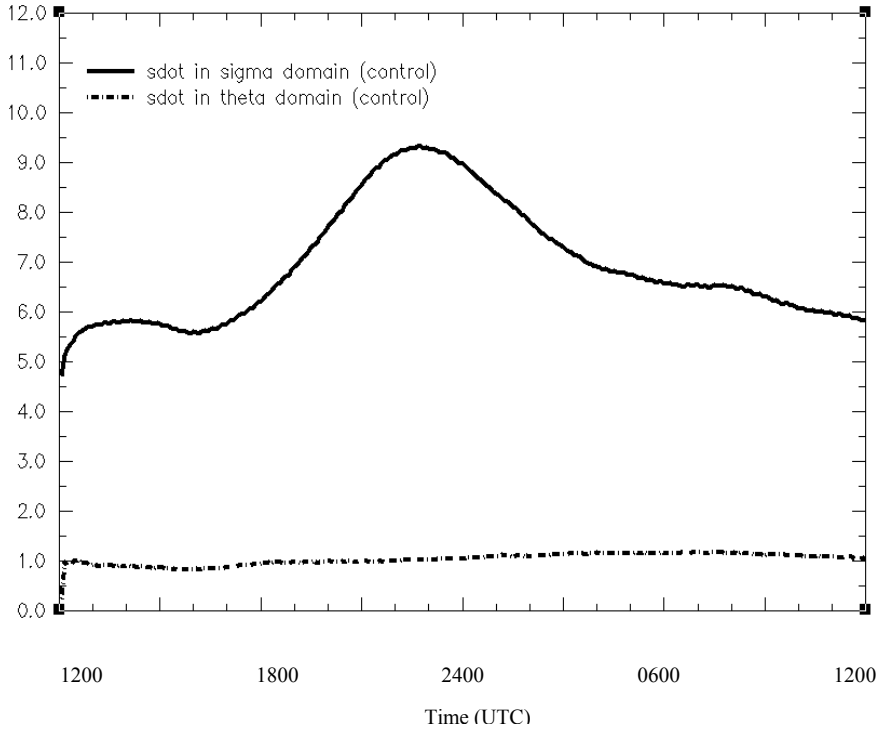

Fig. 9. Mean absolute cross-coordinate vertical transport for May 2000 Exp 1 (control – hybrid vertical coordinate) stratified into sigma vs. theta parts of the domain and averaged over vertical levels.

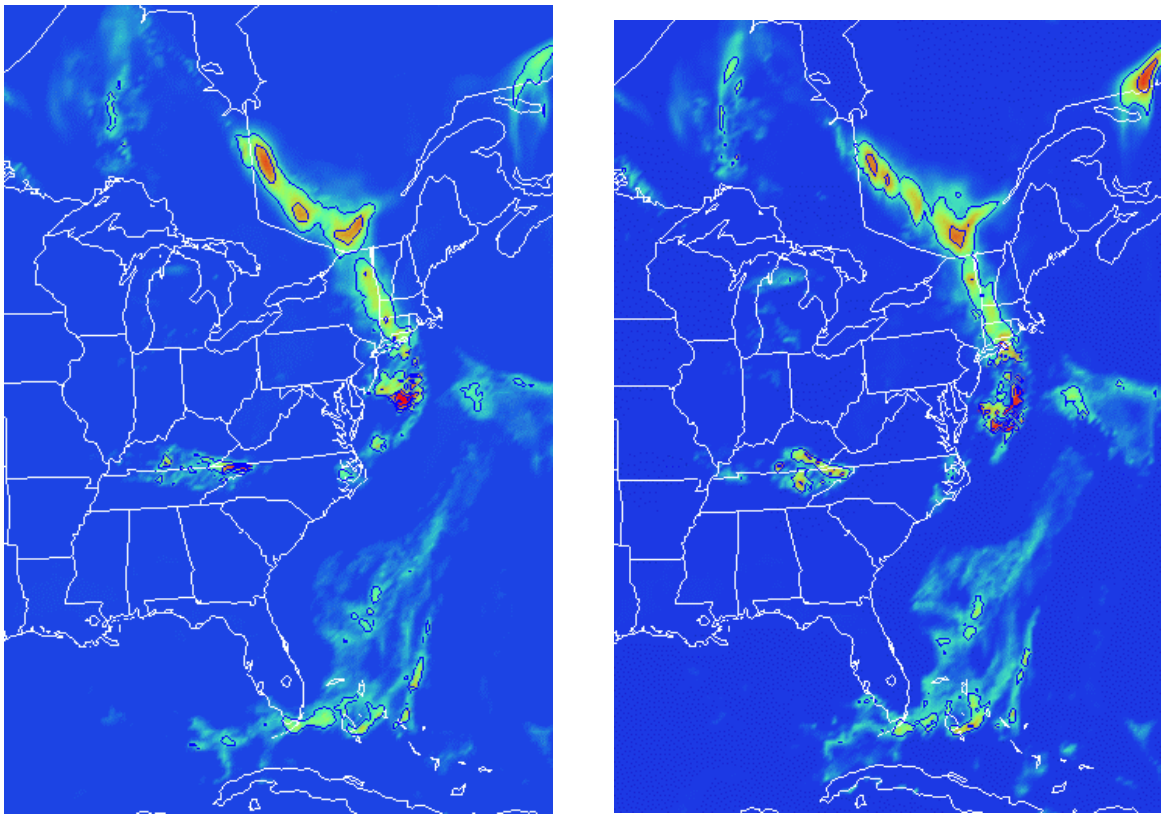

Fig. 10. 3-h precipitation for 0900 – 1200 UTC 24 May 2000 for forecasts initialized at 1200 UTC 23 May. For Exp. 1 (hybrid - left) and Exp. 3 (fixed - right). Contour interval is 0.5 cm per 3 h.

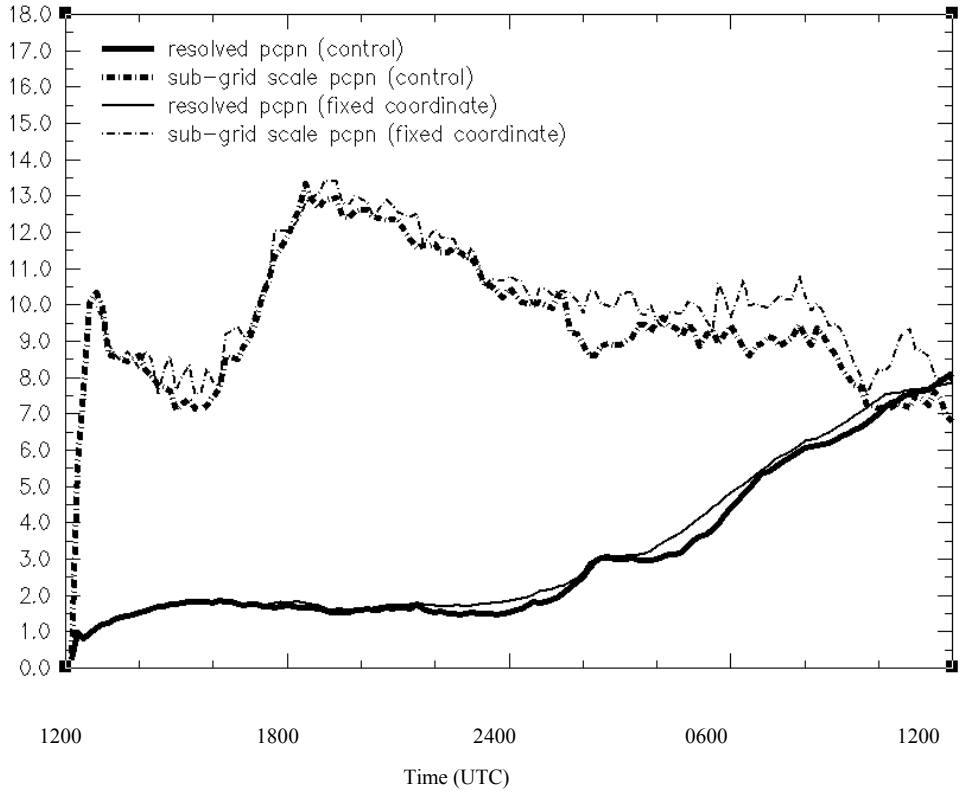

Fig. 11. Averaged precipitation (resolved and sub-grid-scale) over domain for May 2000 Experiments 1 (control) and 3 (fixed sigma). Units = 0.001 mm per 10 min. Horizontal axis is time over 24-h period.

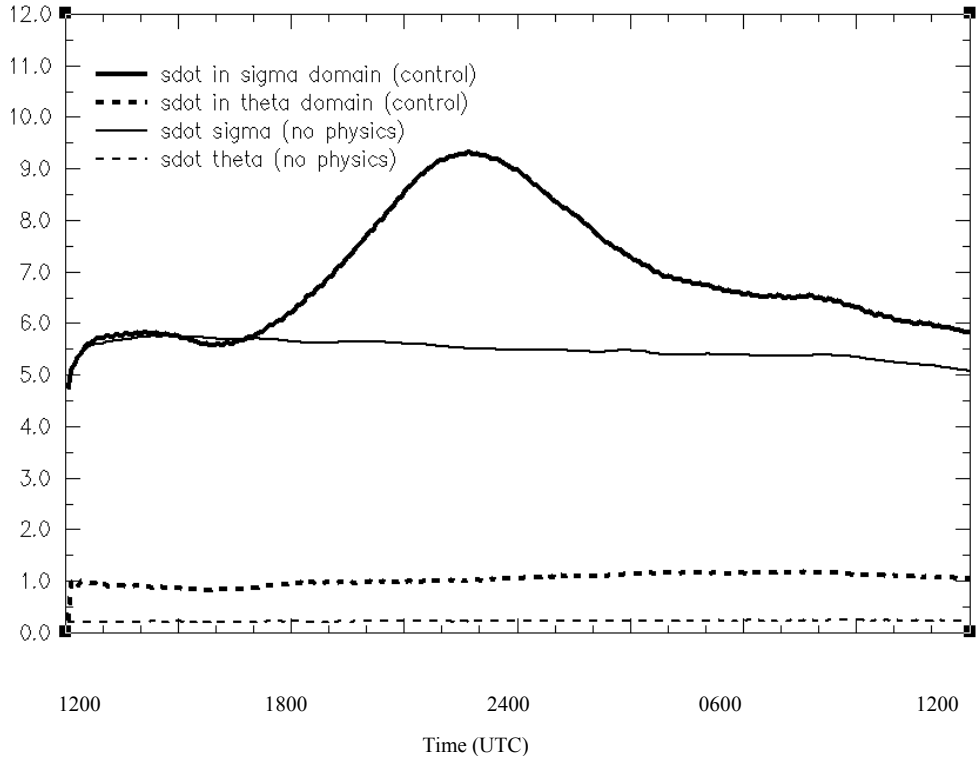

Fig. 12. Mean absolute cross-coordinate vertical transport for Exp 1 (control – hybrid including full moist and boundary-layer physics) and Exp 2 (hybrid with no moist or boundary-layer physics). Values are plotted for both sigma and theta parts of the domain and averaged over vertical levels.

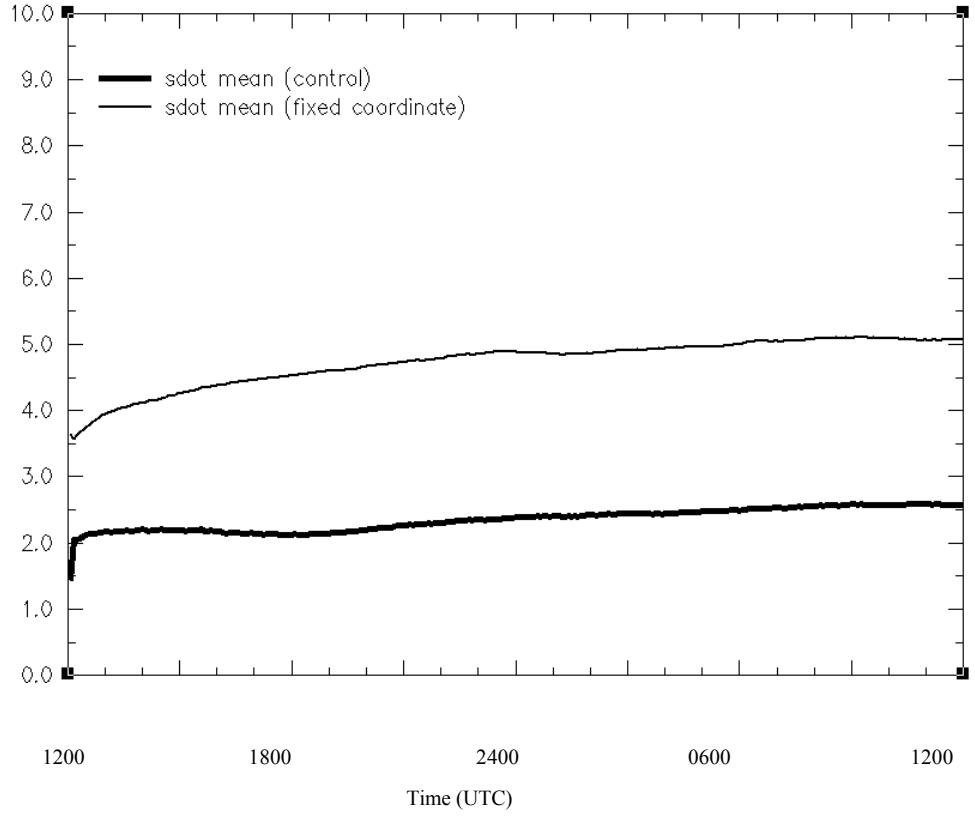

Fig. 13. Same as Fig. 8, but for winter case (8 February 2001).

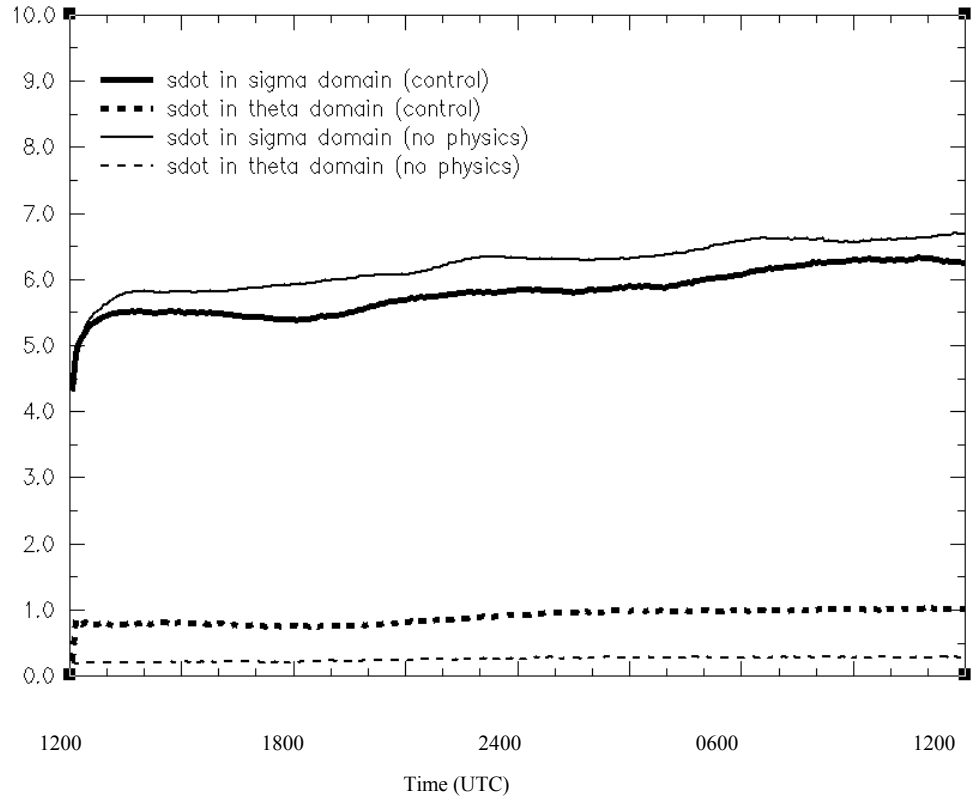

Fig. 14. Same as Fig. 12, but for winter experiment.

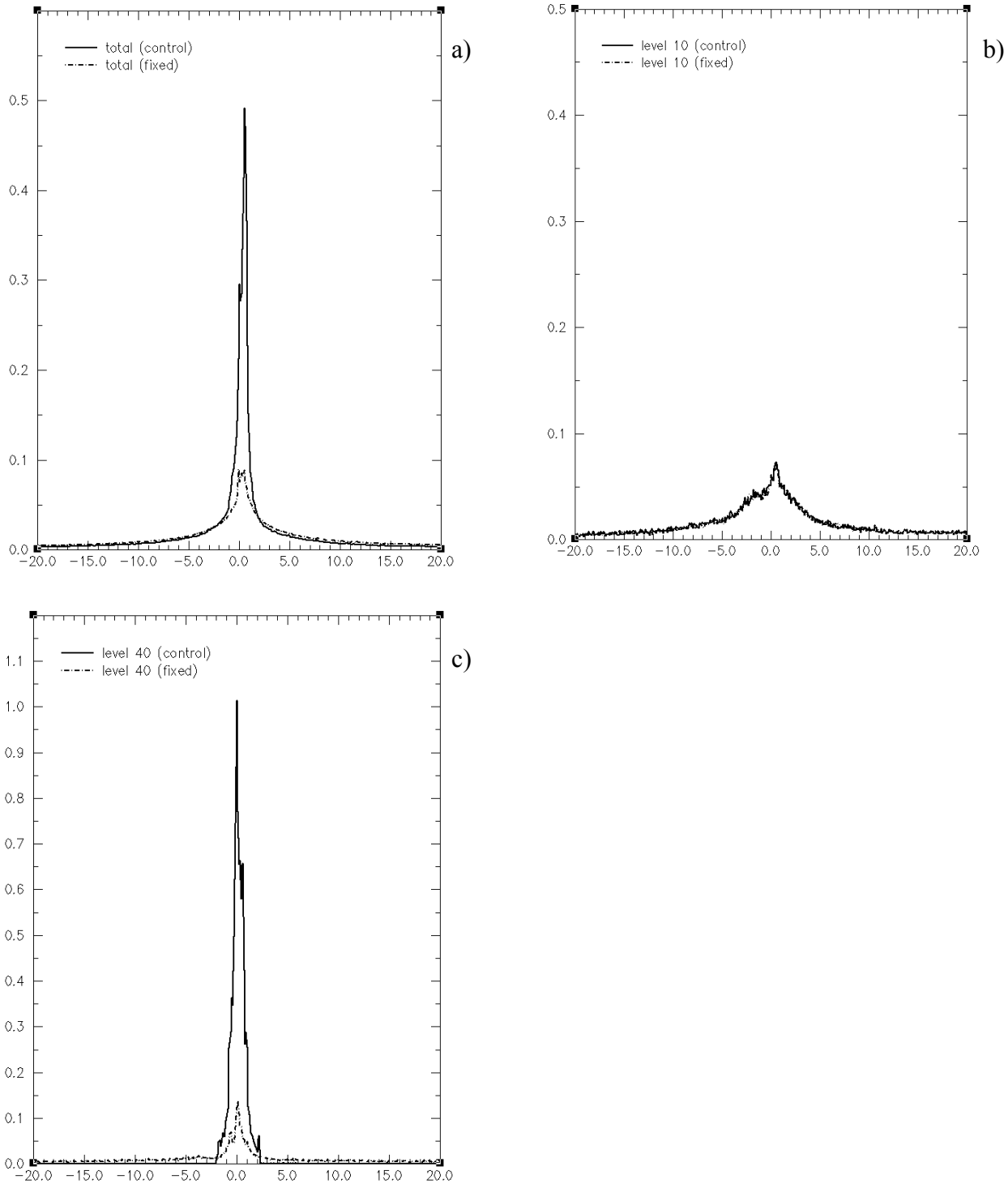

Fig. 15. Empirical relative frequency distributions, probability density function (PDF) of simulated differences of equivalent potential temperature (θ_e) and proxy θ_e from RUC θ-σ (solid) and σ (dashed) versions for 24-h forecasts from warm-season case initialized at 1200 UTC 23 May 2000.

Bin width is 0.1 K, vertical axis is PDF, and horizontal axis is temperature difference in K. a) All levels combined, b) level 10 only, and c) level 40 only. Note different vertical scales for each figure.

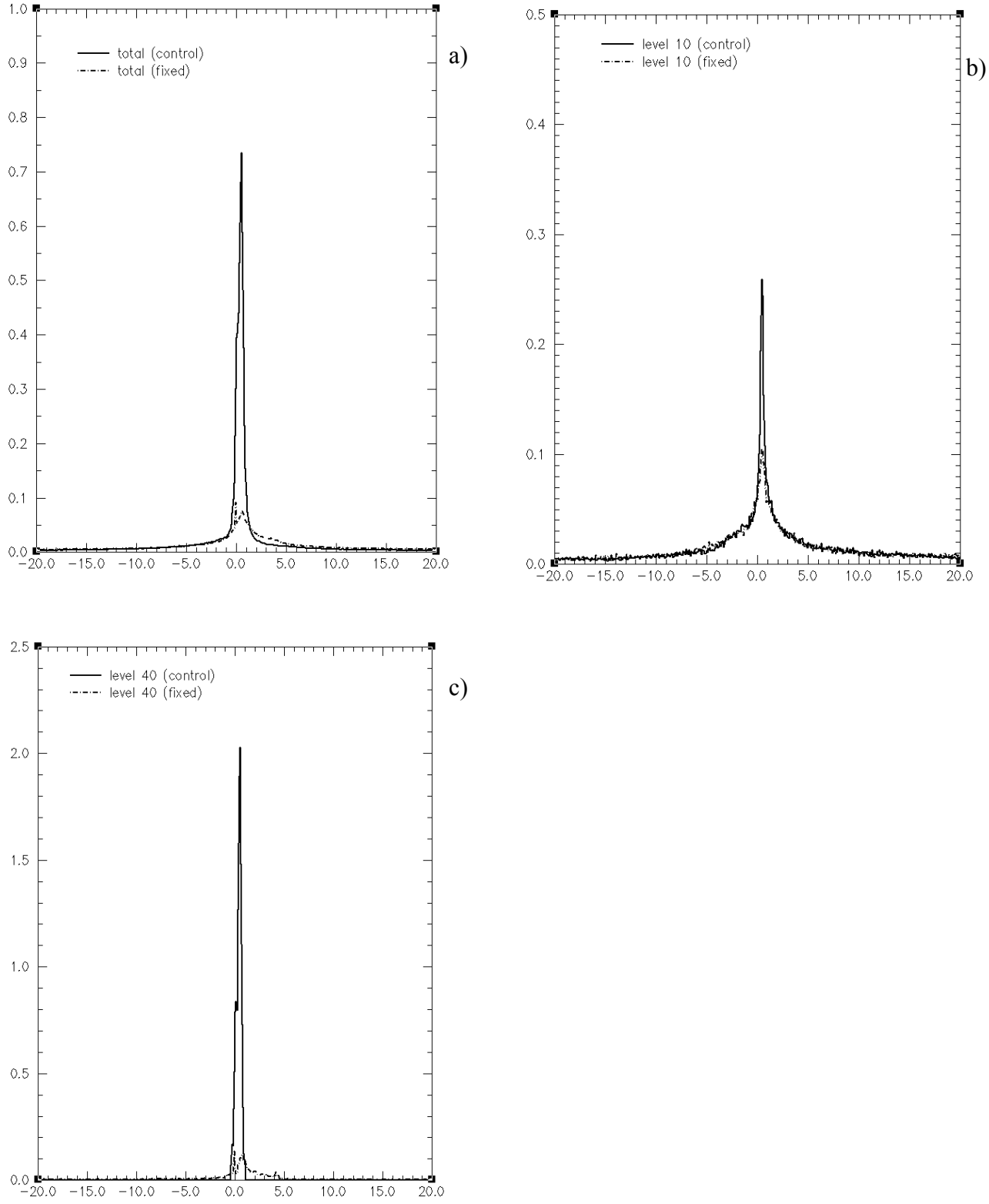

Fig. 16. Same as Fig. 15 but for cold-season case, 24-h forecast initialized at 1200 UTC 8 February 2001.

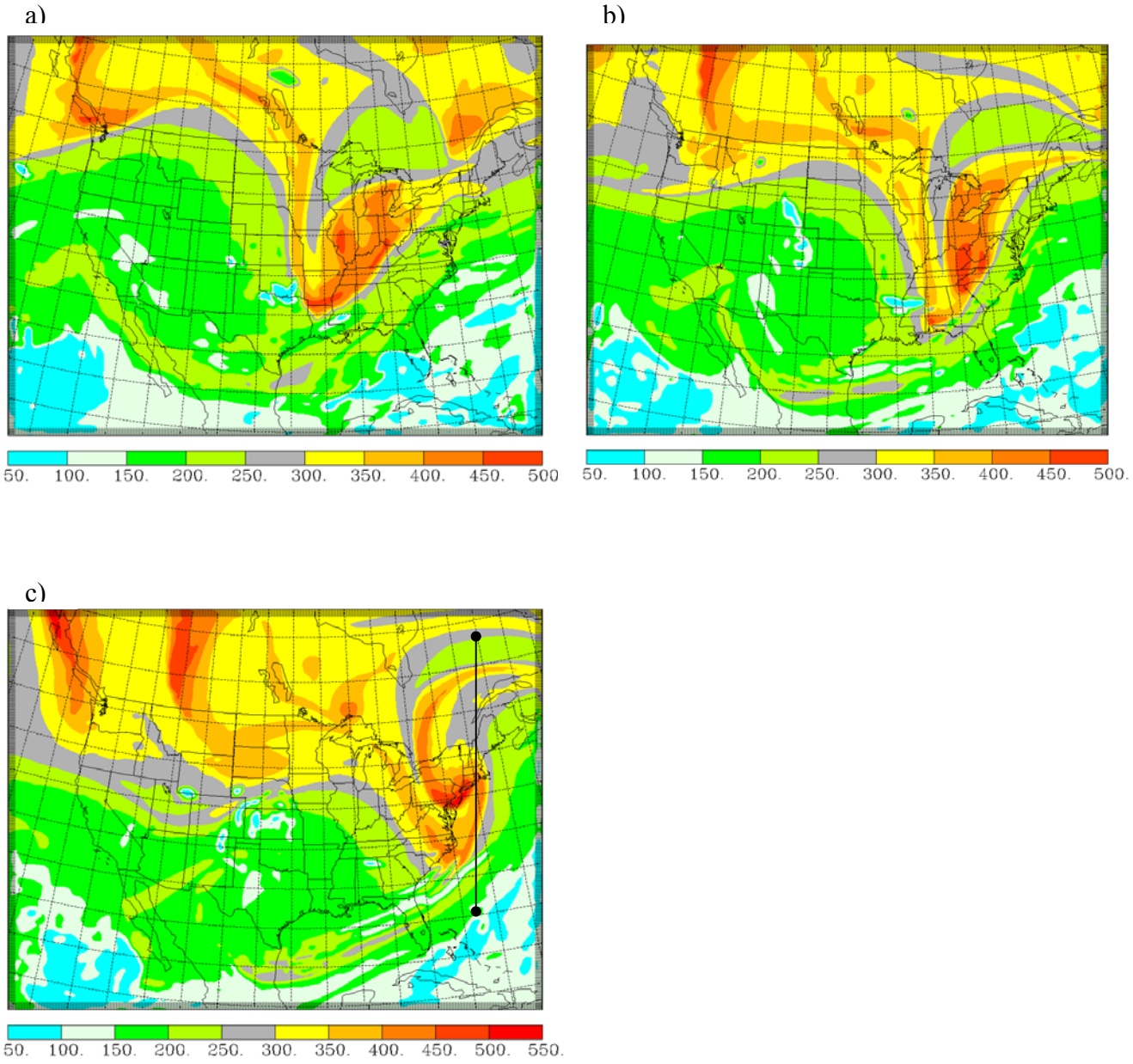

Fig. 17. Pressure (hPa) of the dynamic tropopause (defined in text) from 20-km RUC forecast initialized at 1200 UTC 4 February 2001. a) 12-h forecast, b) 24-h forecast, c) 36-h forecast. Line through eastern part of domain is location of vertical cross sections shown in Fig. 20.

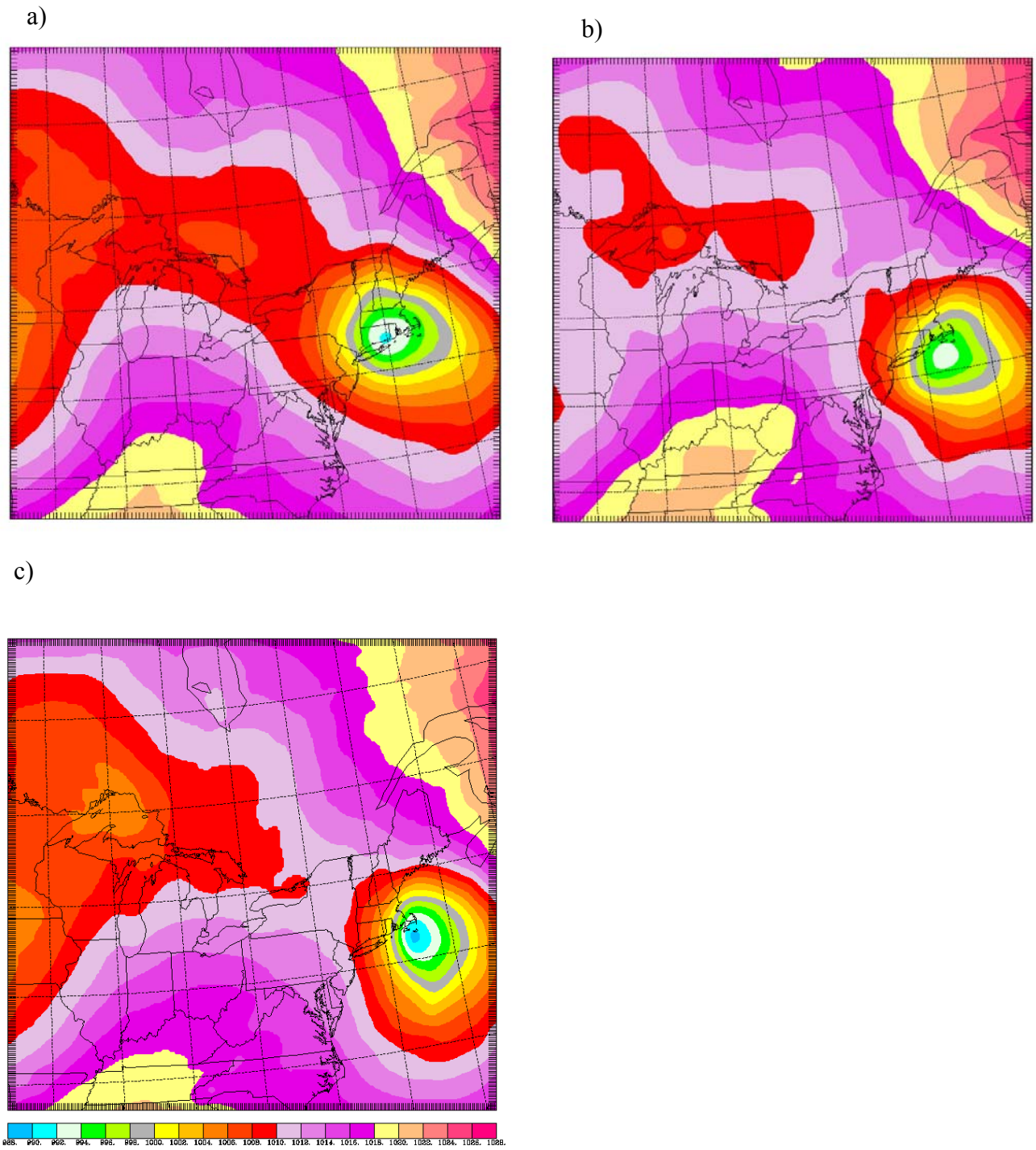

Fig. 18. Sea-level pressure (hPa) valid at 0000 UTC 6 February 2001 for a) 36-h forecast from 20-km RUC, b) analysis from 20-km RUC, c) 36-h forecast from 10-km RUC.

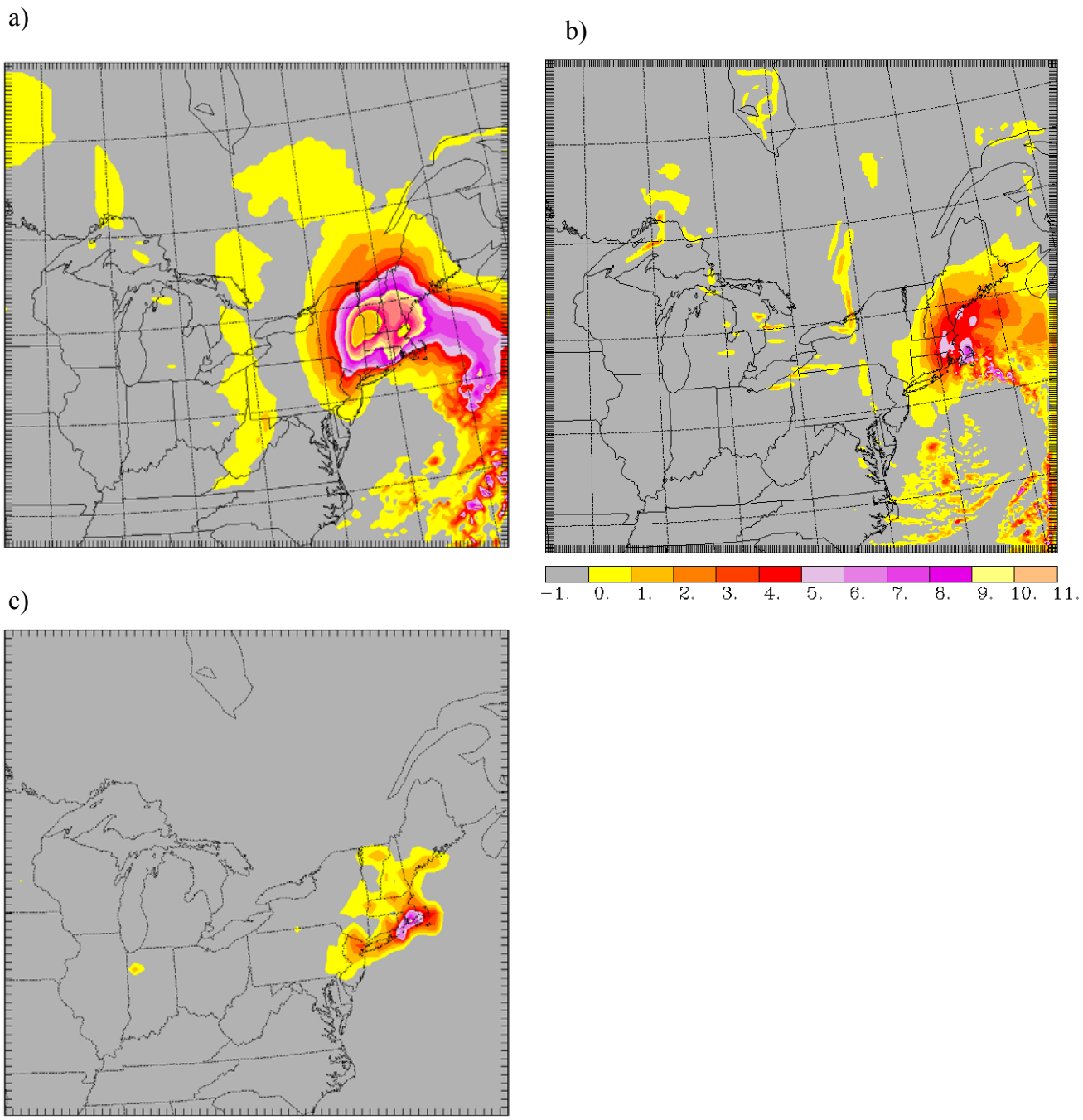

Fig. 19. Estimates of 3-h precipitation (mm) for 2100 UTC 5 Feb – 0000 UTC 6 February 2001 from a) 36-h forecast from 20-km RUC, b) 36-h forecast from 10-km RUC, and c) Stage IV precipitation estimate from gauge and radar data.

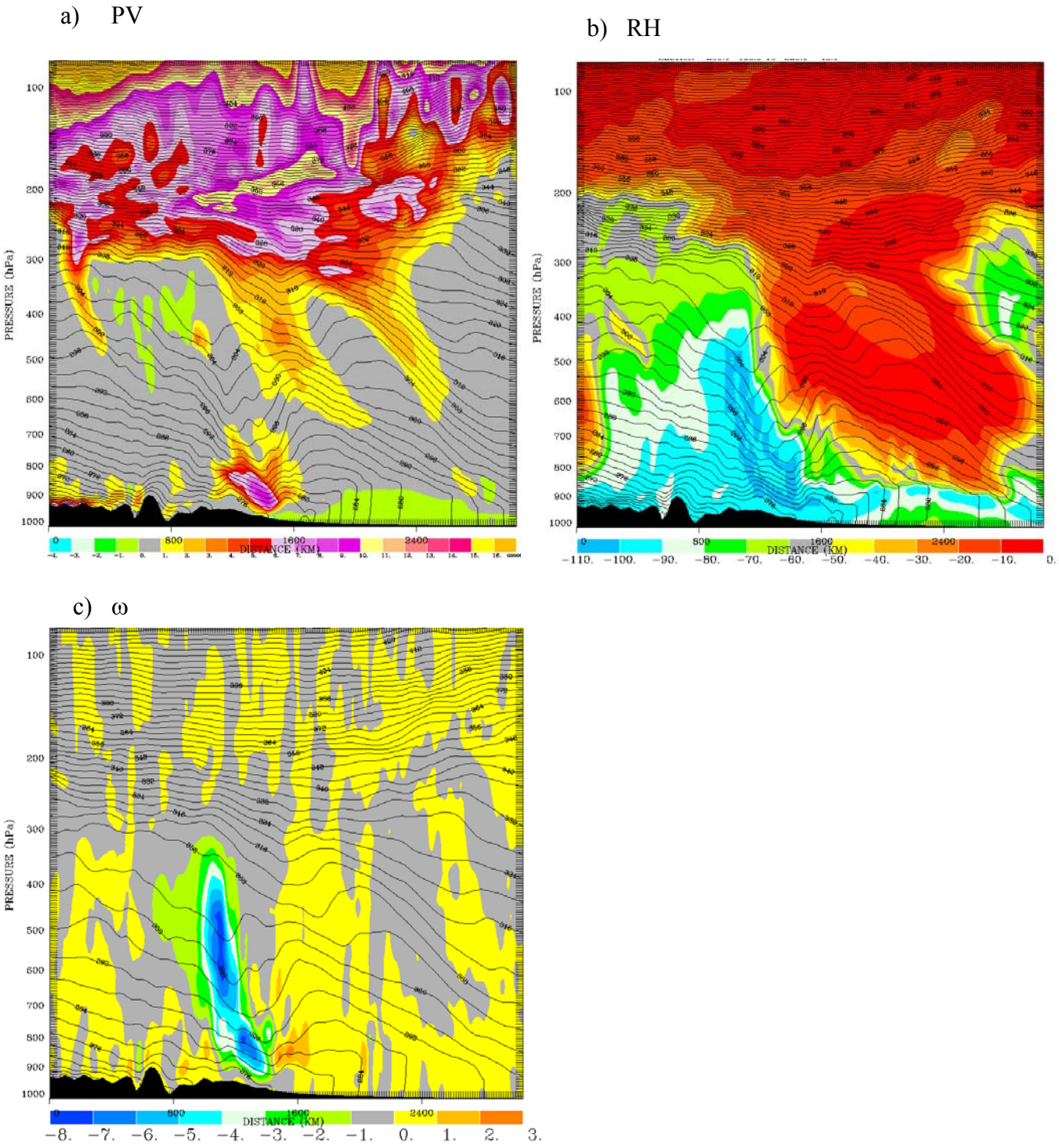

Fig. 20. Vertical cross sections from 36-h forecasts from 20-km RUC model along north-south line shown in Fig. 17c for potential temperature (solid lines, every 4 K) and a) potential vorticity (PVU), b) relative humidity (%), and c) vertical velocity (× 10 μb s^{-1}; -7 = -70 μb s^{-1}).